Quantifying the Extent of Ligand Incorporation and the Effect on Properties of TiO2 Thin Films Grown by Atomic Layer Deposition Using an Alkoxide or an Alkylamide

Maxime Dufond, Maïmouna W Diouf, Clémence Badie, Carine Laffon, Philippe Parent, Daniel Ferry, David Grosso, Jacques C S Kools, Simon D Elliott, Lionel Santinacci

▶ **To cite this version:**

Maxime Dufond, Maïmouna W Diouf, Clémence Badie, Carine Laffon, Philippe Parent, et al.. Quantifying the Extent of Ligand Incorporation and the Effect on Properties of TiO2 Thin Films Grown by Atomic Layer Deposition Using an Alkoxide or an Alkylamide. Chemistry of Materials, 2020, 32 (4), pp.1393-1407. 10.1021/acs.chemmater.9b03621 . hal-02523927

HAL Id: hal-02523927
https://hal.science/hal-02523927

Submitted on 29 Mar 2020

HAL is a multi-disciplinary open access archive for the deposit and dissemination of scientific research documents, whether they are published or not. The documents may come from teaching and research institutions in France or abroad, or from public or private research centers.

L'archive ouverte pluridisciplinaire **HAL**, est destinée au dépôt et à la diffusion de documents scientifiques de niveau recherche, publiés ou non, émanant des établissements d'enseignement et de recherche français ou étrangers, des laboratoires publics ou privés.

Quantifying the Extent of Ligand Incorporation and the Effect on Properties of TiO_2 Thin Films Grown by Atomic Layer Deposition Using an Alkoxide or an Alkylamide

Maxime E. Dufond,[†] Maïmouna W. Diouf,[†,‡] Clémence Badie,[†] Carine Laffon,[†] Philippe Parent,[†] Daniel Ferry,[†] David Grosso,[¶] Jacques C. S. Kools,[‡] Simon D. Elliott,[§] and Lionel Santinacci*[,†]

† *Aix-Marseille Univ., CNRS, CINaM, Marseille, France*

‡ *Encapsulix SAS, Simiane-Collongue, France*

¶*Aix Marseille Univ, Université de Toulon, CNRS, IM2NP, Marseille, France*

§*Schrödinger Inc., New York, USA*

E-mail: lionel.santinacci@univ-amu.fr

Abstract

Atomic Layer Deposition (ALD) of TiO_2 thin films on a Si substrate has been investigated using titanium isopropoxide (TTIP) and tetrakis(dimethylamino)titanium (TDMAT) in combination with water. The deposition rate and the chemical stability of the films are significantly different depending on the Ti precursor and process temperature (T_{ALD}). A significant thickness shrinkage when the films are annealed is

reported for the first time on TiO_2. Comprehensive analysis of the films with XPS, FTIR, ellipsometry and porosimetry demonstrates that some precursor ligands are incorporated (most likely as isopropanol) when ALD is performed at low temperature (i. e. $T_{\mathrm{ALD}} < 200°\mathrm{C}$) using TTIP. The trapped ligand molecules can be removed by annealing, but make the film porous and thus have a detrimental effect on the dielectric properties. Higher quality non-porous films are grown by using TTIP at $T_{\mathrm{ALD}} \geq 200\,°\mathrm{C}$ or by using TDMAT. It is shown that measuring the refractive index is a simple, non-destructive and reliable way to determine film quality. Numerical simulations of ligand coverage show that the measured growth rates are consistent with a self-limiting ALD mechanism, albeit with partial incorporation of ligands from TTIP at low temperature ($T_{\mathrm{ALD}} < 200\,°\mathrm{C}$), which renders part of the surface inactive towards growth. Aside from this, the higher growth rate of TDMAT is due to more desorption of ligands during the Ti precursor pulse. The overall decrease in growth rate with temperature is related quantitatively to decreasing coverage of hydroxyl groups on TiO_2. Comparing the TTIP and TDMAT processes in this way reveals new aspects of the gas-surface chemistry during self-limiting ALD and how this affects film morphology and electrical properties.

Introduction

Titania is present in numerous commercial products such as pigments, paints, sunscreens and toothpastes. Its use is now expanded to sensor, energy and environmental fields of applications.[1] Though a large research effort is devoted to the nanosized structures (e. g. nanoparticles or nanotubes), TiO_2 thin films are also highly interesting because the material exhibits a good chemical stability, a high dielectric constant, a high refractive index (n), and a transparency in the visible and near-infrared range. Those properties are attractive for a variety of applications in electronics, optics, and catalysis.[2] Such thin films can be grown by physical or chemical vapor deposition (CVD) as well as by sol-gel approaches (see e. g. Refs.[3,4]) but only atomic layer deposition (ALD) leads to uniform, compact and conformal ultra-thin layers.

Initially, ALD of TiO_2 has been carried using $TiCl_4$,[5,6] titanium isopropoxide (TTIP),[7,8] titanium ethoxide[9] and TiI_4.[10] Later, the process based on tetrakis(dimethylamino)titanium (TDMAT) has become widespread.[11–13] Though they are much less used, heteroleptic compounds like amino-alkoxides ($Ti(NMe_2)_2(dmae)_2$ and $Ti(NMe_3)_3(dmap)$),[14,15] mixed alkoxide-cyclopentadienyls ($CpTi(OMe)_3$)[16] and alkoxide-amidinates/amides ($Ti(OiPr)_3$(NiPr-Me-amd) and ($Ti(NMe_2)_2(OiPr)_2$))[17] were also successfully applied to grow TiO_2 thin films. The oxygen source was mainly H_2O but it is also possible to pulse a more reactive compound such as H_2O_2[10,18] or O_3.[19,20] Plasma-enhanced ALD (PE-ALD) has also been successfully employed with a mixture of N_2 and O_2.[21] Gas bubbling in the canister[22] or liquid injection have been applied to enhance the Ti precursor transport to the surface. This latter approach has been used for TTIP[23] and tris-(dimethylamido)-mono-(N,N'-diisopropyl-dimethyl-amidoguanidinato)-titanium (TiA_3G_1).[2] More recently, solution-phase ALD has been reported for TTIP and H_2O successively injected over the substrate in diethyl ether, exhibiting a similar behavior to the equivalent vapor phase process.[24]

This abundant literature shows that numerous ALD recipes lead to the formation of TiO_2 layers (see Ref.[25] for an extensive review). The present study focusses though on TTIP and

TDMAT because they are by far the most frequently-used Ti precursors and also because the properties of the deposited layers from these two precursors can be significantly different. Such discrepancy is frequently ascribed to the incorporation of carbonaceous ligands in the layers when using the alkoxide. DFT studies on the ALD of TiO_2 have shown that Ti-O bond formation is required for protonated alkoxide ligands to desorb.[26] Similar computations have revealed that metal-oxide densification reduces the barriers for protonated amide ligands to desorb from a HfO_2 surface.[27] However, it has not yet been clearly established how this sort of chemical behavior in gas-surface reactions ultimately affects the properties of the films that are deposited. For instance, carbonaceous impurities in an as-deposited film are often assumed to be due to ligand decomposition in parasitic CVD reactions, especially at elevated temperature, but could such impurities also be the result of incomplete desorption in ALD? One of our goals is to establish whether the observed growth characteristics are consistent with self-limiting ALD-style reactions, or whether less controllable CVD of this sort is playing a role. We also seek to explain the temperature dependence of growth and film properties, including whether an "ALD window" is observed.

In this paper, after the description of an unexpected discrepancy between the deposition rates and chemical stabilities depending on the Ti precursor, an exhaustive comparison of the morphology, the composition and the structure of the films grown using the alkoxide and the alkylamide is reported. This reveals new insights into the deposition process, which evidently depends on the chemical nature of the Ti precursors as well as on the subsequent thermal treatment. Numerical analysis of film thickness and coverage of intermediates then yields an explanation in terms of the chemical processes occurring at the surface during deposition. A correlation between n and the electrical performance demonstrates the strong impact of precursor chemistry on the ALD process and subsequently on the final dielectric properties of the layers.

Experimental

Surface preparation and ALD of TiO_2

TiO_2 deposition was performed on Si (100) (Sil'tronix ST). The wafers were cut in $1.5 \times 1.5\,cm^2$ squares and degreased by sonicating in acetone, ethanol, and ultrapure water. The native oxide layer was removed by a dip in HF 10 % for 30 s. The samples were then vigorously rinsed in water, dried under a nitrogen stream and stored in an Ar-filled glovebox.

The TiO_2 thin films were grown by ALD in a Fiji 200 reactor from Veeco/Cambridge Nanotech using TTIP (98%, Strem Chemicals) or TDMAT (99%, Strem Chemicals) as Ti precursors and ultrapure water as oxygen source. The TTIP and TDMAT canisters were heated at 80 °C while the water tank was left at room temperature. The reaction chamber temperature (T_{ALD}) was ranged from 70 to 250 °C to study its impact on the deposition. The ALD cycle consisted, for both Ti precursors and H_2O, of sequential pulse, exposure and purge steps. During the exposure phase, the chamber is isolated from the pumping system to allow for a higher residence time of reactants in the chamber. This mode is generally used to conformally coat high aspect ratio substrates. The pulse, exposure and purge durations were 2:7:15 s for Ti precursors and 0.2:7:15 s for water. The comparison with literature[7,13] indicates that the exposure mode and the long steps of the sequence lead to the saturation of the surface (i. e. the deposition occurs under the ALD regime) and a uniform film growth. The growth per cycle (GPC) vs. the precursor pulse duration is plotted for TDMAT, TTIP and water in Figure S1 of the supporting information. They indicate that the selected pulse times correspond to a saturation situation. The number of ALD cycles (N) was varied to adjust the thickness of the TiO_2 films (t).

After the TiO_2 deposition, an annealing step was performed in air at various temperatures ($T_a = 100$ to 450 °C) and durations (up to 2 hours) in order to transform the amorphous layer to anatase and to remove the ligands that could have been trapped in the film. Four types of samples have thus been studied depending on the precursor nature (TTIP or TDMAT) and

if the films are as-grown (AG) or annealed (An). To facilitate their designation, in following, they are named: TTIP-AG, TTIP-An, TDMAT-AG or TDMAT-An.

Characterization methods

The thickness and refractive index of the TiO_2 thin films were measured by spectroscopic ellipsometry using a M-2000 V (J. A. Woollam Co.). The curve fitting (Ψ and Δ) was performed with the CompleteEase software applying a Cauchy oscillator model. The roughness (R_{RMS}) of the layers was not implemented in the simulation. Atomic force microscopy (AFM) has indeed revealed that the films exhibit a very small roughness ($R_{\mathrm{RMS}} \approx 0.5\,\mathrm{nm}$) that could be neglected (see AFM images presented in Figure S2 of the supporting information). Note that no cracks appeared after annealing in the films. This was, however, observed by Iancu et al.[28] when annealing is performed at higher temperatures (T_{a} >500 °C). It is attributed to the O_2 incorporation into the film.

The chemical stability of the films grown under various conditions have been tested by immersing the samples in 1 M KOH. Such a corrosive solution does not react with the TiO_2 itself but etches the Si underneath rapidly. This allows detection of porosity or permeability of the films.

The crystalline structure of the TiO_2 layers was analyzed using a high brilliancy rotating anode, Rigaku RU-200BH equipped with a Xenocs Fox3D Cu 12_INF mirror, Osmic, and an image plate detector, Mar345 (Rayonix). The radiation used was Cu Kα, $\theta = 1.5418$Å and the beam size was $0.5 \times 0.5\,\mathrm{mm}^2$. The experimental resolution was about 0.3° in 2θ.

Scanning and Transmission Electron Microscopies (SEM, TEM) were used to investigate the morphology, the thickness, and the crystalline structure of the TiO_2 layers using a JEOL JSM 6340F, JEM 2010 and a JEM 3010. The TEM cross sections were carried out on samples prepared by ion milling with a precision ion polishing system (PIPS, Gatan M691). The thickness measurements were used to calibrate the ellipsometric measurements.

The chemical composition of the TiO_2 thin films was analyzed by X-ray photoelectron

spectroscopy (XPS) using a Resolve 120 hemispherical electron analyzer with a pass energy of 20 eV and a Mg K_α radiation source at 1253.6 eV (PSP Vacuum). Survey spectra and high-resolution spectra of the C 1s, O 1s, and Ti 2p core-level regions were collected at a take-off angle of 60°. Data processing was performed using the CasaXPS analysis software using a Shirley-type background, component peaks defined by binding energy (BE), full width at half maximum (FWHM) and Gaussian/Lorentzian envelopes. The carbon containing species trapped in the layer were monitored by Fourier transform infrared (FTIR) spectroscopy with a resolution of 4 cm^{-1} in the wavenumber range of 900 to 3800 cm^{-1}. Measurements were achieved by using a MIRacle (PIKE Technologies) attenuated total reflectance (ATR) accessory mounted in a Vertex 70 spectrometer (Bruker) equipped with a DLaTGS detector.

The porosity was investigated by environmental ellipsometry porosimetry (EEP) using a M-2000V spectroscopic ellipsometer equipped with a controlled atmosphere cell in which relative humidity (RH) was regulated as reported in details earlier.[29]

Electrical measurements were performed on metal-oxide-semiconductor (MOS) structures fabricated by evaporating successively 10/100 nm thick Cr/Au dots ($\varnothing = 500\mu$m) on *ca.* 40 nm thick ALD TiO_2 thin films. The back contact to the Si electrodes was established by smearing InGa eutectic. The current-voltage curves were obtained using a Modulab Ammeter/DC voltage source equipped with a low current amplifier module (Solartron Analytical).

Computational method

Isolated gas-phase molecules were computed at the density functional theory (DFT) level using the Jaguar code.[30] Electronic structure was computed using the Perdew Burke Ernzerhof functional[31,32] and LAV3D** basis set,[33,34] converged to an energy change $< 5\times10^{-5}$ E_H and RMS density matrix change $< 5\times10^{-6}$, and hence molecular structures were optimized freely using redundant internal coordinates until energy changes were $< 5\times10^{-5}$ E_H and RMS gradient changes were $< 3\times10^{-4}$ atomic units.

Results and discussion

Growth rate, annealing and etching of the films

The growth rate of TiO_2 was investigated depending on the Ti precursor nature. Figure 1a shows the GPC against T_{ALD} for both TTIP and TDMAT. The thickness was measured by spectroscopic ellipsometry. The presented GPCs are extracted from the thickness vs. N linear plots where at least 4 points were reported. It appears first that the GPC values and their evolution against T_{ALD} are different depending on the Ti precursor. When pulsing TTIP, the so-called ALD window is located between 90 and 200°C while the GPC is significantly higher for TDMAT that, however, does not exhibit a well-defined ALD window since the deposition rate continuously decreases with the T_{ALD}.

The shaded areas plotted on the background of Figure 1a correspond to the GPC ranges reported in literature for both precursors. The comparison indicates that the present data are in line with previous works (see detailed plots with references in Figure S3 in supporting information). In the case of TTIP, the present GPC is, however, one of the highest reported (ca. 0.35 Å/cycle between 90 and 200°C). This could be attributed to the use of the exposure mode that leaves sufficient time for the molecules to diffuse and react with all the available surface sites. The continuous GPC decrease measured for TDMAT with increasing process temperature was also seen by Xie et al.,[13] who showed with DFT that this could not be accounted for by the desorption of intermediates. The other explanation that they mention is a decrease of hydroxyl coverage on the growing TiO_2 surface with temperature, and the chemical growth mechanism described later in this paper quantifies how the observed growth is consistent with such a decrease.

The GPC after the usual annealing step is also plotted (dashed lines) against the process temperature on Figure 1a for both precursors. While it remains unchanged for TDMAT, the deposition rate is significantly lower after the thermal treatment when the TiO_2 is grown at

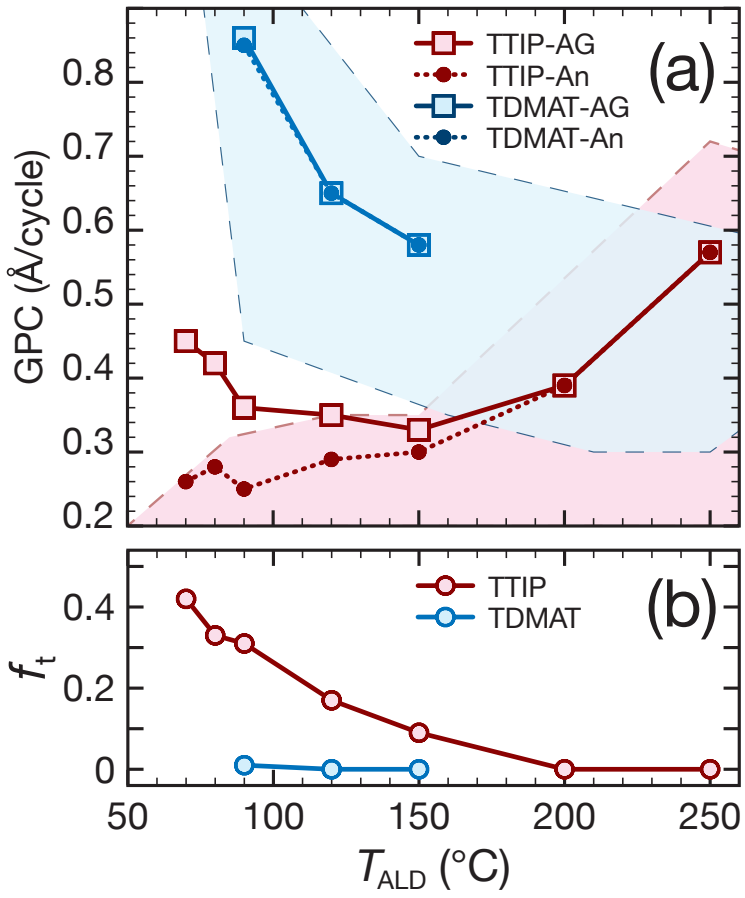

Figure 1: (a) Evolution of the GPC for ALD of TiO_2 at various T_{ALD} using TTIP (red) and TDMAT (blue) prior to (squares) and after (circles) a 2 h annealing at 450 °C in air. The shaded red and blue areas correspond to the GPC found in the literature (full values and references can be found in Figure S3 in supporting information). (b) Fraction of thickness loss (f_t) during the annealing process of layers.

low T_{ALD} using TTIP. This effect corresponds to a shrinkage of the film thickness after the annealing. The ratio between the initial thickness (t_{AG}) and the thickness after annealing (t_a) is called the fraction of thickness loss (f_t) and is defined according to Eq. (1):

$$f_t = \frac{t_{AG} - t_a}{t_{AG}} \quad (1)$$

It is plotted on Figure 1b where it can be seen that the shrinkage decreases with T_{ALD} and it vanishes at $T_{ALD} = 200°C$. While it commonly occurs on hybrid films grown by molecular layer deposition (MLD),[35,36] this effect has been less documented for pure ALD processes. It has been observed during ALD of Al_2O_3,[37,38] but no example could be found for TiO_2. In the case of non-continuous TiO_2 layers grown by atmospheric pressure chemical vapor deposition using TTIP[39] a 16% thickness loss has been reported. It was ascribed to the film sintering. During such an annealing process, it is well-known that the initial amorphous TiO_2 layer is transformed to polycrystalline anatase and if the temperature is sufficiently high to rutile or brookite (more details will be given hereinafter).[28] A thickness increase has even been observed on films grown using TDMAT at $T_{ALD} = 200°C$ when the annealing is performed in pure O_2 at $T_a > 500°C$.[28] This phenomenon should proceed independently of the Ti precursor. The phase transformation is not primarily responsible for the layer shrinkage because the densities of the as-deposited and annealed layers, measured by X-ray reflectivity (see Figure S4 in Supplementary Information), are very close ($\approx 3.7\,g{\cdot}cm^{-3}$). This is in agreement with the densities of amorphous TiO_2 and anatase reported in literature (3.60-3.80 and 3.84-3.90 $g{\cdot}cm^{-3}$, respectively[40,41]). One can therefore suspect a precursor condensation at low temperature or an incomplete reaction during the ALD. In both cases, TTIP ligands would be trapped in the film during the deposition process and then removed during the thermal treatment. The ligand insertion has already been observed during an in situ XPS investigation[42,43] and by in situ surface-enhanced Raman spectroscopy (SERS).[44] However, here we give the first evidence of ligand removal after thermal treatment.

Since the TiO_2 layers are often grown to protect a surface,[45,46] the chemical stability has been assessed in an agressive alkaline solution (1 M KOH). The SEM top views presented in Figure 2 show the surface after immersion for different ALD conditions. The surface covered by TiO_2 grown at low T_{ALD} using TTIP is strongly damaged (Figure 2a). At several locations, the film is either swelled or fully detached. Conversely, when the samples are annealed or

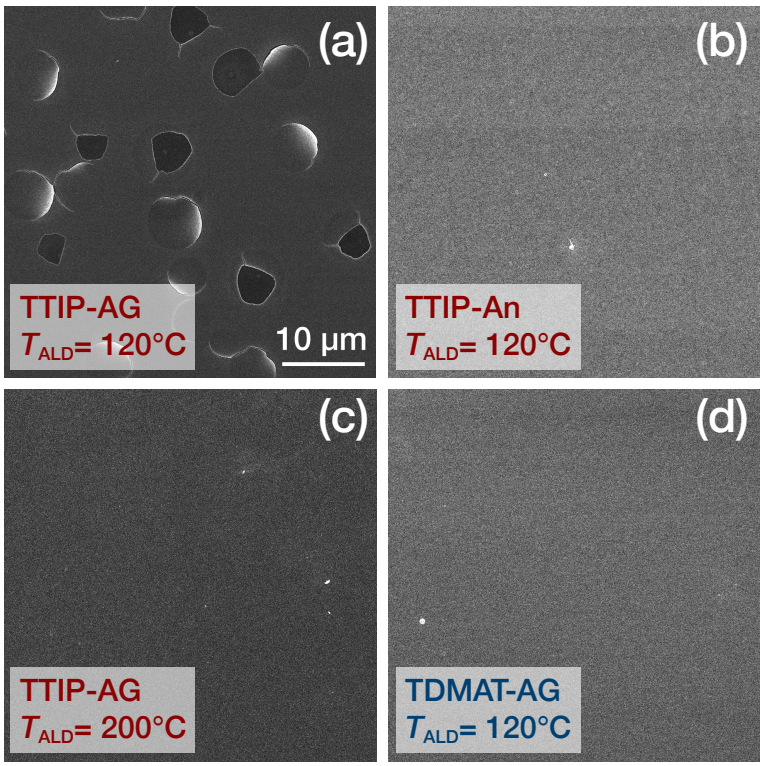

Figure 2: SEM top views of TiO_2 layers grown on Si using TTIP (a,b,c) or TDMAT (d) after immersion in 1 M KOH for 5 min (a,b) and 10 min (c,d). The T_{ALD} is indicated on the images and an annealing at 450°C in air is performed in (b).

when the deposition has been performed at higher temperature (i. e. $T_{ALD} = 200$°C) the films are fully protective (Figure 2b and 2c). No detrimental effect of the immersion in KOH is also observed for the thin films grown with TDMAT (Figure 2d). TiO_2 is, in fact, known to be stable at such high pH[47] while the underlying Si is strongly etched in KOH (through the ultrathin native SiO_2). The swelling of the TiO_2 layers corresponds therefore to the

accumulation of H_2 generated during the dissolution of the substrate according to Eq. (2).[48]

$$Si + 2H_2O + 2OH^- \longrightarrow Si(OH)_4^{2-} + H_2 \longrightarrow SiO_2(OH)_2^{2-} + 2H_2 \quad (2)$$

When the amount of H_2 is too high the film cracks and can be lifted off (Figure 2a). The film instability is solely observed for TTIP-AG at low T_{ALD}. This corresponds to the conditions causing the layer thinning ($f_t > 0$). This indicates that the instability of the film is related to the shrinkage occurring after the thermal treatment. To explain this phenomenon, one can assume that the films grown at low temperature using TTIP are porous and/or contain compounds that can react with the solution. Further morphological, structural and chemical analyses have thus been performed to elucidate this phenomenon. Note that the purities of the precursors indicated in the experimental section are very close (98 and 99% for TTIP and TDMAT respectively) and cannot induce such differences.

Evolution of the crystalline structure and morphology

The crystalline structure of the TiO_2 layers has been studied by XRD and TEM. Though the amorphous-to-anatase phase transformation appears for $T_a \geq 350°C$[49] (see the evolution of the diffractograms with T_a on Figure S5 of supporting information), the annealing has been performed at $T_a = 450°C$ to shorten the treatment duration. Figure 3 shows the X-ray patterns before and after the annealing for TTIP and TDMAT. As shown in a previous work,[50] after the ALD process, both precursors lead to amorphous films while crystalline peaks corresponding to anatase are observed on the diagrams after the thermal treatment. The crystalline structures after annealing are very similar showing that the type of the Ti precursor does not play a significant role in the crystallization process. Note also that the deposition temperature has an impact on the crystalline structure. For $T_{ALD} \geq 200°C$, the diffractograms show weak peaks corresponding to anatase (see Figure S6 in supporting information). This is enhanced when the deposition is carried out at 250°C. Similar observations

have been reported before using TTIP.[51] TEM cross sectional views of the TiO_2 films grown

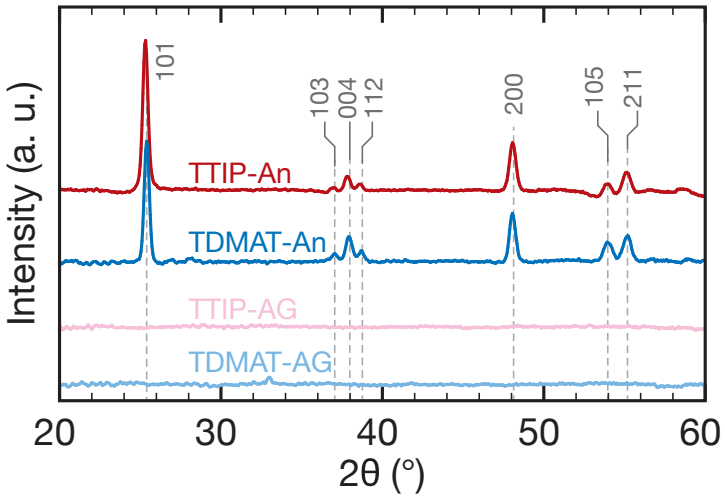

Figure 3: X-ray diffractograms of TiO_2 layers grown using TTIP and TDMAT at $T_{ALD} = 120°C$ before and after annealing at $T_a = 450°C$ for 2 h. The diffraction peaks corresponding to the anatase are indicated on the plot (according to JCPDS card # 00-021-1271).

at $T_{ALD} = 120°C$ are shown in Figure 4. In all cases, the native SiO_2 layer that covers the Si is observed at the interface between the substrate and the deposit. The apparent difference in thickness of the SiO_2 films is an artefact of the imaging. This is due to the TEM observation itself and does not correspond to a real discrepancy. The film thicknesses measured by TEM (Figures 4a, 4b and 4c) are in line with the ellipsometric measurements. This validates therefore the GPC values plotted in Figure 1. The shrinkage after the thermal treatment is also confirmed by comparing the t values in Figure 4a and 4b. The thickness of the annealed sample (43±2 nm) is indeed 19% lower than the as-grown sample (53±3 nm). Due to the high N_2/O_2 concentration ratio (ca. N_2/O_2; 78:21 vol. %), the annealing in air does not lead to O incorporation and the subsequent volume expansion. This is in agreement with the study of the effect of the thermal treatments in pure O_2 and pure N_2.[28] As expected from the XRD investigations, the high magnification TEM images (Figures 4d, 4e and 4f) show that the TTIP-AG sample is amorphous while both TTIP-An and TDMAT-An exhibit clearly a polycrystalline structure (TEM cross sections of TDMAT-AG are very similar to TTIP-AG. They are shown in Figure S8 of the supporting information). The large crystalline domains

observed on Figures 4e and 4f reveal the high quality of the films. (It can be noted that the domains seems to be qualitatively larger in size for TDMAT). In all cases, the layers look quite homogeneous and not porous. Figure 5 shows a TEM cross section from deposition at

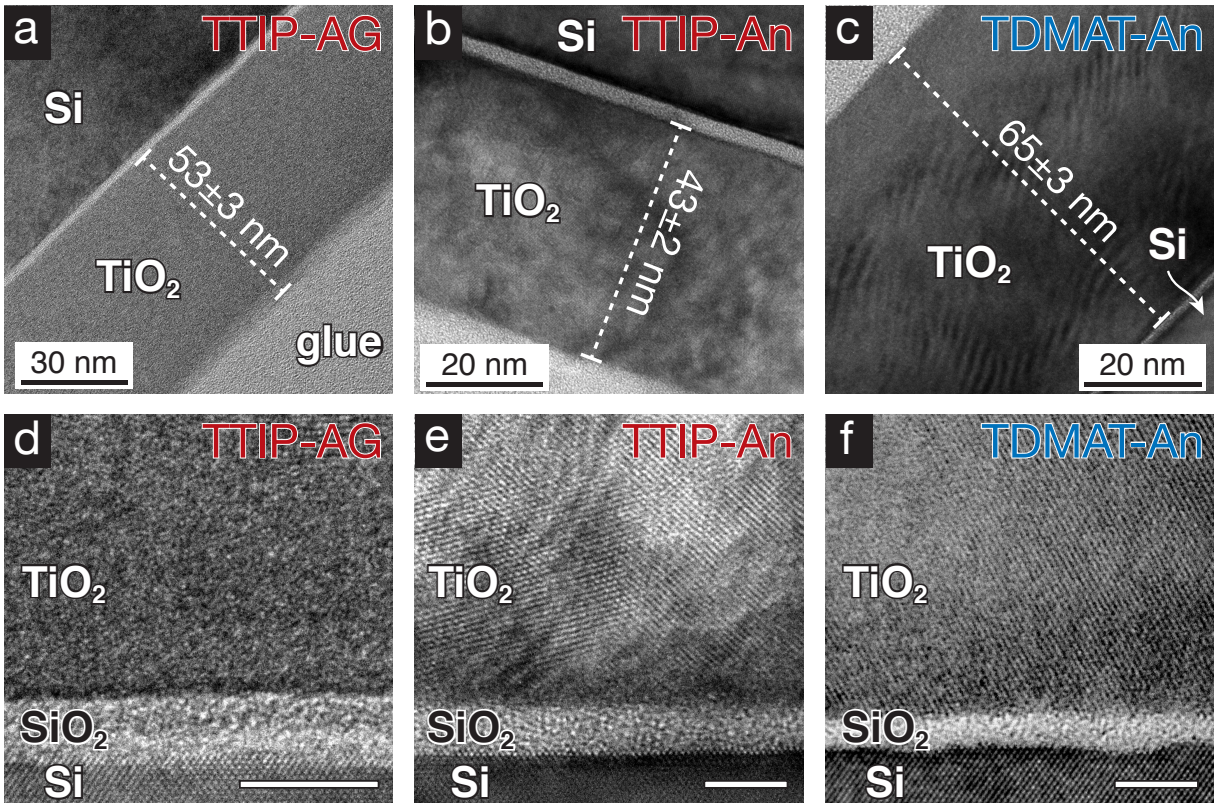

Figure 4: TEM cross sections of TiO_2 layers grown on Si ($T_{ALD} = 120\,°C$) at low and high magnification: (a,d) TTIP-AG ($N = 1500$ cycles), (b,e) TTIP-An ($N = 1500$ cycles) and (c,f) TDMAT-An ($N = 1000$ cycles). The scale bars on (d,e,f) correspond to 5 nm.

$T_{ALD} = 70°C$ and annealing at 450°C. At such high magnification, it is possible to distinguish small areas ($\varnothing \approx$ 2-3 nm) where the crystalline lattice seems altered. These features could in principle be attributed either to beam-induced modification of the specimen or to nanoscaled pores. However, since no similar distortions have been observed on TiO_2 layers grown at higher temperatures (see e. g. Figure 4), we conclude that this is not an effect of the electron irradiation, but rather indicates a very fine-grained porosity of the film.

Note that the TiO_2 films grown at $T_{ALD} = 70°C$ were easily removed by the tweezers when manipulating the samples. Conversely no adhesion issues were observed for layers grown at higher process temperatures. No deeper investigations have been carried on this point since

the mechanical integrity of the deposits was qualitatively satisfactory.

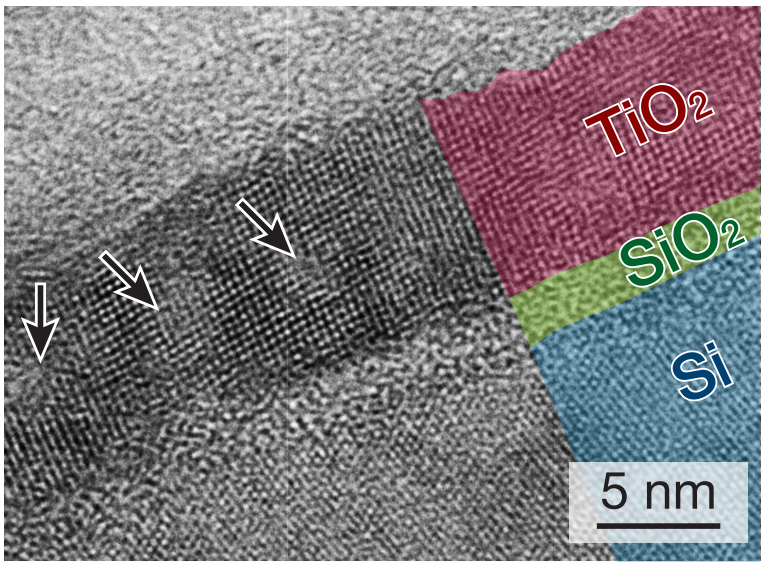

Figure 5: High magnification TEM cross section of a TiO_2 layer grown on Si at $T_{ALD} = 70\,°C$ after annealing at $T_a = 450°C$ for 2 h ($N = 300$ cycles). The arrows show where the lattice appears to be altered, as referred to in the text.

Composition of the films

Chemical analysis has been performed by XPS on three different types of TiO_2 layers grown at $T_{ALD} = 120°C$: TTIP-AG, TTIP-An and TDMAT-AG. The XPS survey for TTIP-AG (Figure 6a) confirms the expected composition of the film: mainly titanium and oxygen with some additional carbon. A similar composition is deduced from the survey spectra for TTIP-An and TDMAT-AG (these survey spectra are shown on Figure S7 in the supporting information). The Ti 2p and C 1s core-levels for as-grown TiO_2 layers using TTIP are plotted in Figures 6b and 6c, respectively. The decomposition of Ti 2p leads to Ti $2p_{3/2}$ and Ti $2p_{1/2}$ peaks located at 459.2 and 464.9 eV, respectively, with a spin-orbit splitting of 5.7 eV. This corresponds to the typical signature for stoichiometric TiO_2.[52,53] The C 1s region shows four contributions, noted C_I (285.1 eV), C_{II} (286.3 eV), C_{III} (287.15 eV) and C_{IV} (289.2 eV), that can be ascribed to C–C, C–O, C=O and O–C=O bonds, respectively. These contributions are not only due to the expected surface contamination but also to TTIP ligands

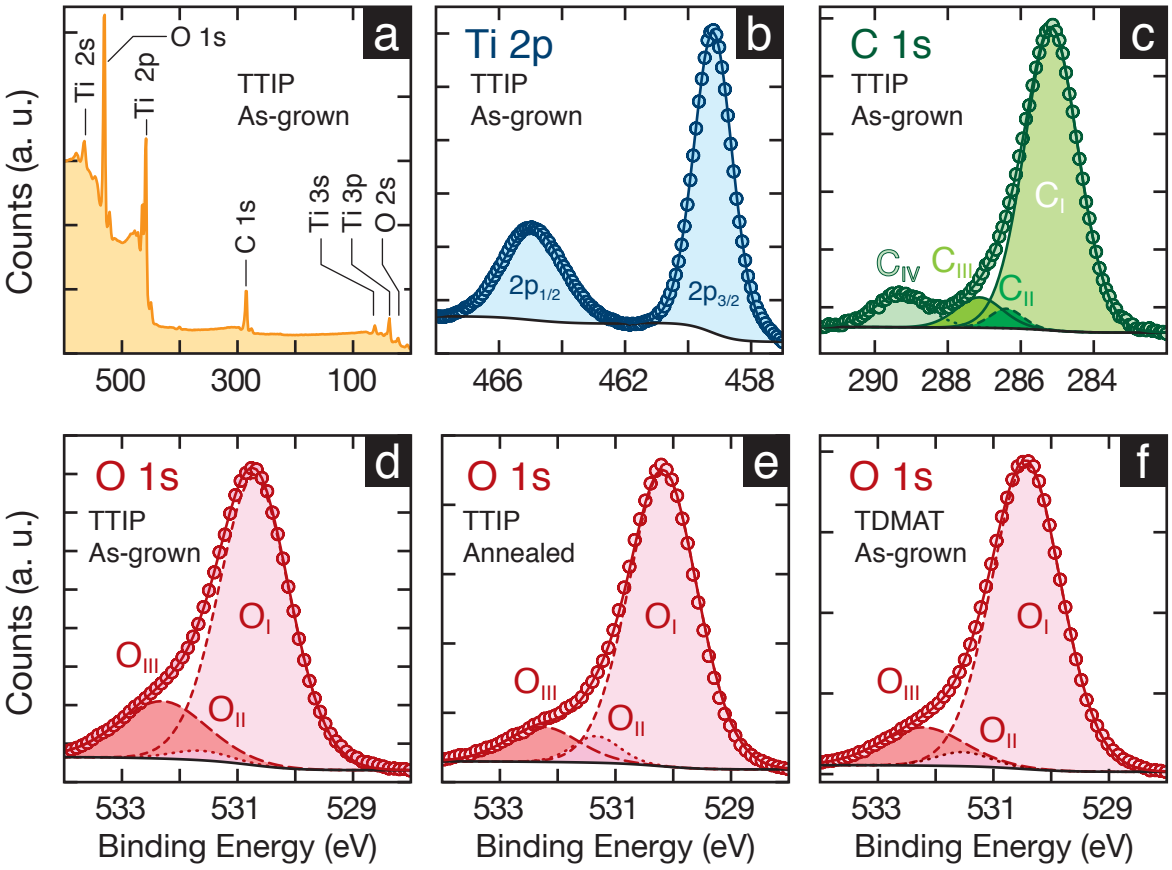

Figure 6: Chemical analysis of TiO_2 films depending on the Ti precursor (TTIP or TDMAT) prior to and after annealing. (a) Survey spectrum, (b) Ti 2p peak and (c) C 1s peak using TTIP without annealing. (d, e, f) comparison of the O 1s peak region for TTIP-AG, TTIP-An and TDMAT-AG, respectively.

that have been apparently incorporated into the TiO_2 film as reported earlier.[43,53] Since very similar results are obtained for TTIP-An and TDMAT-AG, one has to investigate the O 1s region of the three types of layers to compare the amount of ligands that are possibly trapped during the ALD process. Figures 6d, 6e and 6f show the O 1s core-level spectra for TTIP-AG, TTIP-An and TDMAT-AG, respectively. In all cases, the decomposition is performed using three contributions denoted O_I (530.3 eV), O_{II} (531.7 eV), O_{III} (532.2 eV). The low energy peak O_I is assigned to the Ti–O bond while O_{II} and O_{III}, at higher binding energies, correspond to C–O and –OH bonds.[43] O_{II} and O_{III} are thus related to the surface contamination but also to the remaining precursor ligands stuck in the film. The quantitive analysis of the O 1s peaks, shown in Table 1, allows for comparing the $O_I/(O_I+O_{II}+O_{III})$ ratio that stems from the TiO_2 contribution with respect to additional oxygen contributions on different samples. Conversely $O_{II}+O_{III}$ corresponds to the surface contamination that should be constant on all samples and to the amount of carbonaceous compounds included in the TiO_2 films. Although O_I never reaches 100% because surface contamination is always present, the comparison of $O_{II}+O_{III}$ demonstrates that TTIP-AG layers contain more ligand residues (21.5%) than the same films after annealing (TTIP-An: 15.6%) or when an the alkylamide is used (TDMAT-AG: 15.7%).

Complementary chemical analysis has been carried out by FTIR spectroscopy. Figure 7a presents the comparison of the absorbance of TiO_2 layers grown using TTIP ($N = 1500$ cycles, $T_{ALD} = 90$ and 200°C) and TDMAT ($T_{ALD} = 90$°C, $N = 600$ cycles) without thermal post-treatment. Five different spectral regions are identified on the TTIP-AG. Weak vibrational bands at 1110 and 1170 cm^{-1} correspond respectively to the C–O symmetric and antisymmetric stretching modes in the isopropoxide ligand,[19,54] while the weak absorptions of the C–H bending modes from the alkyl chain are detected between 1380 and 1500 cm^{-1}.[54] The band exhibiting a medium intensity at 1700-1780 cm^{-1} is ascribed to the C=O stretch and intense bands located between 2800-3000 cm^{-1} stem from the C–H stretch of the alkane chain. Finally the broad band ascribed to the O–H stretch located between 3100-3700 cm^{-1}

Table 1: Quantitative analysis of the O 1s core-level spectrum depending on the precursor nature and thermal treatment.

Samples	Assign.	BE (eV)	FWHM	At. %
TTIP-AG	O_I	530.7	1.4	78.5
	O_{II}	531.6	1.2	2.1
	O_{III}	532.3	1.8	19.4
TTIP-An	O_I	530.2	1.4	84.4
	O_{II}	531.3	1.0	5.1
	O_{III}	532.3	1.5	10.5
TDMAT-AG	O_I	530.4	1.4	84.3
	O_{II}	531.5	1.1	3.1
	O_{III}	532.2	1.7	12.6
TDMAT-An	O_I	530.4	1.5	84.4
	O_{II}	531.5	1.1	5.2
	O_{III}	532.2	1.8	10.4

corresponds to an alcohol function or to hydroxyl groups incorporated in the film or adsorbed onto the surface. It could also be ascribed to water but the samples were deaerated for long-time to get rid of it. The spectrum of TTIP-AG at low T_{ALD} exhibits numerous similarities with titanicone and alucone films grown by MLD.[35,36] The observed contributions indicate therefore that some ligands of the TTIP are trapped in the TiO_2 layer during the deposition process. The chemical signature is close to that of isopropanol, which is usually obtained after hydrolysis of the isopropoxide. Rahtu et al.[55] have previously proposed that the isopropoxide ligands react into either isopropanol, acetone, diisopropyl ether, and/or propene, the most likely being isopropanol. The absorption band around 1780 cm^{-1} is attributed to a carbonyl group that could arise from the oxidation of the alcohol. However when the TTIP process is performed at high temperature ($T_{ALD} = 200°C$) or when TDMAT is used, the FTIR signals corresponding to the ligands are almost negligible. The spectra show only weak absorption bands centered at 2900 cm^{-1} related to C–H stretching.

Figure 7b shows the influence of the thermal annealing on the composition of TTIP-AG ($T_{ALD} = 90°C$). As soon as the annealing proceeds (after 1 min), the FTIR spectrum shows a change of the chemical composition: except for the O–H stretching band, all the absorption

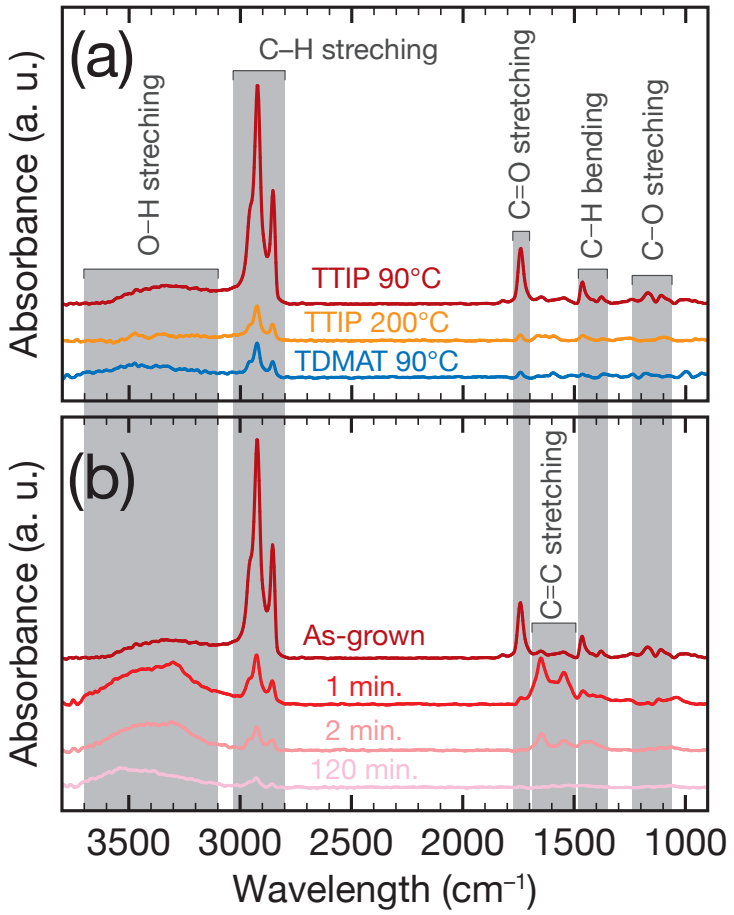

Figure 7: FTIR absorbance spectra of TiO_2 thin films grown on Si. (a) Evolution as function of the Ti precursor and T_{ALD} for as-grown films. (b) FTIR absorbance spectra as a function of the annealing duration for TTIP at $T_{\mathrm{ALD}} = 90°\mathrm{C}$.

bands are significantly quenched and an additional signal, corresponding to C=C stretching, is detected between 1500-1700 cm^{-1}. This can be attributed to the dehydration of the alcohol group leading to an alkene (see Eq. 3). Hackler et al. have recently shown the formation of propene by in situ SERS[44] during ALD of TiO_2 from the isopropoxy ligands of the TTIP or from the trapped isopropanol. According to Carrizosa et al. such a reaction is catalyzed by the TiO_2.[56]

$$R{-}CHOH{-}CH_3 \xrightarrow{\Delta} R{-}CH{=}CH_2 + H_2O \tag{3}$$

with $R = CH_3$ in the case of isopropanol. The increase of the broad band at high wavenumbers (3100-3800 cm^{-1}) would therefore correspond to the eliminated water that is still absorbed in the film. After 2 min at $T_a = 450°C$, the intensity of the C=C and O–H stretches start to decrease and the C=C band vanishes after 120 min while the O-H stretch is low. At the end of the annealing, the FTIR spectrum is similar to those obtained with TTIP at $T_{ALD} = 200°C$ or TDMAT at $T_{ALD} = 90°C$, i. e. with almost no embedded ligands. During the annealing process, a large part of the trapped ligands are thus modified and/or carbonized and finally desorbed from the layer.

Optical properties

The optical properties of the TiO_2 thin films have been probed by spectroscopic ellipsometry. Figure 8a shows the variation of n against the process temperature. It is significantly higher when TDMAT is used and, in both cases, n increases linearly with T_{ALD}. At a given wavelength (λ), the n variation is generally related to the evolution of the composition, the crystalline structure and/or the porosity. Since both TTIP-AG and TDMAT-AG films are amorphous (or quasi-amorphous until $T_{ALD} < 250°C$), the different refractive indexes for TTIP or TDMAT as well as their evolution with T_{ALD} cannot arise from the modification of the crystalline structure (this will be confirmed later from Figure 9). The evolution is more probably due to a change of the chemical composition and/or porosity. This is in line with

the chemical analyses shown above (Figures 6 and 7). The linear increase indicates therefore a direct correlation between the ligand content and the refractive index. Note also that the discrepancy between TDMAT and TTIP tends to disappear with T_{ALD} since the slope is steeper for the alkoxide. This convergence is expected because the films exhibiting the same composition should reach the same reference index for TiO_2.

The evolution of n against the annealing temperature is plotted for TTIP on Figure 8b. Though the initial n are different depending on the process temperature ($n_{80°C} = 1.90$ and $n_{120°C} = 2.04$), a linear behavior is also observed in both cases and n saturates to reach the same plateau ($n \approx 2.2$) when $T_a \geq 350°C$. This indicates that the trapped ligands are extracted from the TiO_2 layer during the thermal treatment. This is again in agreement with the chemical analyses shown before (Figures 6 and 7) and numerical analysis (Table 2). Moreover the ellipsometry indicates that, up to the plateau ($T_a \approx 350°C$), the amount of released ligands is linearly dependent on the annealing temperature.

As mentioned above, n varies generally the composition, the crystalline structure and/or

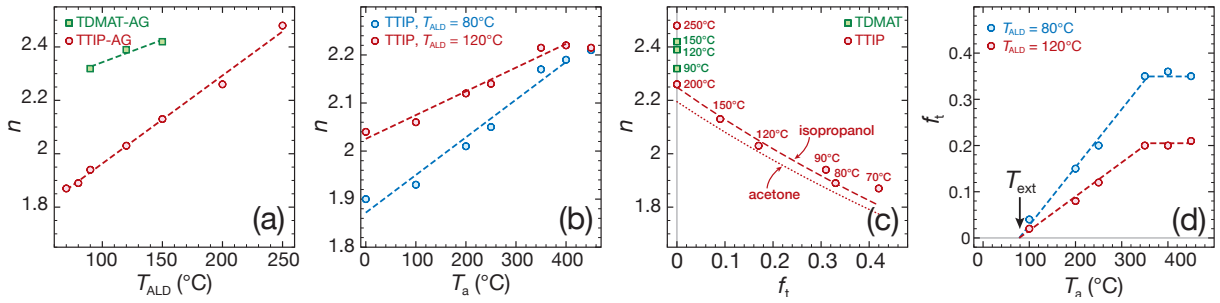

Figure 8: Evolution of n against T_{ALD} (a), T_a (b) and f_t (c) for TiO_2 layers grown using TTIP and TDMAT. The conditions are indicated on the plots. The annealing duration in (b) is 2 h. The corresponding T_{ALD} are also indicated directly on each data point in (c). Evolution of f_t against T_a for TiO_2 thin films grown using TTIP at $T_{\mathrm{ALD}} = 80$ and 120°C (d). $T_{ext} \approx 80°C$ corresponds to the minimum temperature required to extract the trapped ligands.

the porosity. Since n varies mainly at temperatures lower than the phase transformation ($T_a \approx 350°C$) and a plateau is reached when the crystallization proceeds, the rise of the refractive index could be mainly ascribed to a composition change (i. e. the removal of the trapped ligands) and to a compacting of the film (i. e. porosity decrease). This is further

supported by Figure 9 that compares the evolution of n against time and the intensity of the main anatase diffraction peak when a layer containing a large amount of ligands is annealed at the phase transition temperature. Although the two curves reach a plateau after 500 min, significant differences are observed before this. The refractive index rises quickly to its maximum ($n = 2.17$ after 120 min) while the peak intensity shows an initiation delay of 60 min prior to slowly increasing and reaching a plateau after 500 min. The slight decrease of the refractive index after 120 min could, nevertheless, be ascribed to the phase transformation.

Since n varies only when the annealing leads to a film thickness shrinkage (i. e. for

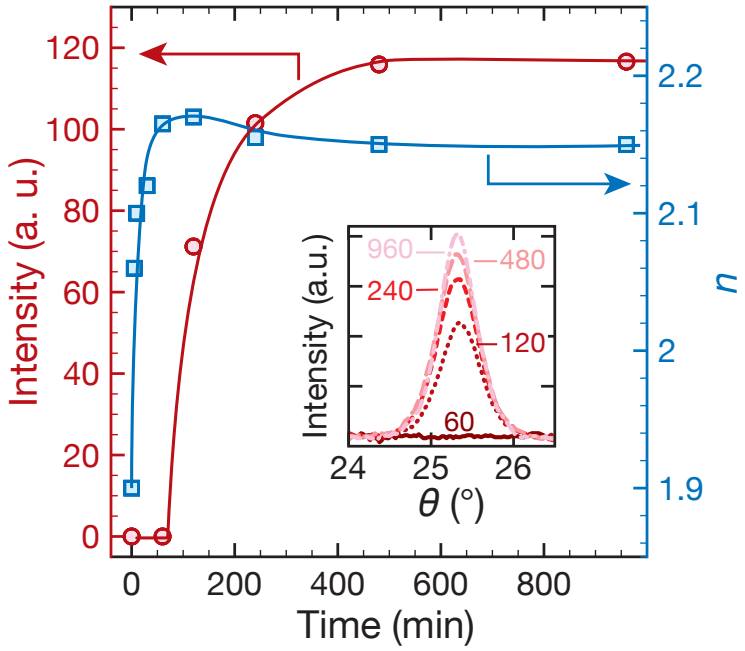

Figure 9: Comparison of the evolution of the (101) diffraction peak intensity (circles) and the refractive index (squares) against the annealing time at $T_a = 350°C$ for a film grown at $T_{ALD} = 80°C$ using TTIP. The inset shows the (101) diffractions for increasing annealing time (the durations are indicated in min. on the inset).

$f_t > 0$), the evolution of n vs f_t is plotted on Figure 8c for TDMAT and TTIP at various T_{ALD}. While n drops with f_t for the alkoxide, it does not exhibit any dependency for the alkylamide. Similarly to Figure 8a, n is high with the TDMAT: it varies between 2.32 and 2.42 because almost no ligands are trapped. The refractive index further increases after annealing to reach 2.48 (not shown here) that corresponds to one of the highest reported

values in literature.[57,58]

In the case of TTIP, except for $T_{\mathrm{ALD}} \geq 200°\mathrm{C}$, n continuously drops with f_{t}. This is expected since Figure 8a demonstrates that n decreases with the amount of embedded ligands. Assuming the fraction of thickness loss is exclusively related to the ligand elimination, it is possible to use the Lorentz-Lorenz effective medium approximation (EMA) to express the refractive index according to the volume fractions of the TiO_2 (ϕ_{TiO_2}) and of the trapped ligands (ϕ_{L}):

$$\frac{n^2-1}{n^2+2} = \phi_{TiO_2}\left(\frac{n_{TiO_2}^2-1}{n_{TiO_2}^2+2}\right) + \phi_{\mathrm{L}}\left(\frac{n_{\mathrm{L}}^2-1}{n_{\mathrm{L}}^2+2}\right) \tag{4}$$

where n_{TiO_2} and n_{L} are the refractive indices of the TiO_2 and of the trapped ligands, respectively. According to the chemical analyses described above, we can easily consider that all the removable ligands have been extracted from the TiO_2 film after the 2 h annealing at 450°C. Therefore, the volume contraction of the film can solely be attributed to the ligand release (the amount of TiO_2 remains unchanged) and one can write the volume occupied by TiO_2 (V_{TiO_2}) and the volume occupied by the ligands (V_{L}) as following:

$$V_{TiO_2} = V_{\mathrm{a}} \tag{5}$$

$$V_{\mathrm{L}} = V_{\mathrm{AG}} - V_{\mathrm{a}} \tag{6}$$

where V_{AG} and V_{a} are, the volumes of the film prior to and after the annealing. The resulting expression shows that the volume fraction ϕ_{L} is equal to f_{t}:

$$\phi_{\mathrm{L}} = \frac{V_{\mathrm{L}}}{V_{TiO_2}+V_{\mathrm{L}}} = \frac{t_{\mathrm{AG}}-t_{\mathrm{a}}}{t_{\mathrm{AG}}} = f_{\mathrm{t}} \tag{7}$$

The effective n can then be expressed as a function of f_{t} by rewriting the Lorentz-Lorenz relation:

$$\frac{n^2-1}{n^2+2} = (1-f_t)\left(\frac{n_{TiO_2}^2-1}{n_{TiO_2}^2+2}\right) + f_t\left(\frac{n_{\mathrm{L}}^2-1}{n_{\mathrm{L}}^2+2}\right) \tag{8}$$

The curves in Figure 8c correspond to Eq. (8) in which $n_{TiO_2} = 2.25$ and $n_L = 1.35$ or 1.38. The refractive index of TiO_2 is used at $f_t = 0$ because it corresponds to the film from which all the removable ligands have been taken out. Some organic species can indeed remain in the layer leading to a refractive index slightly lower than expected for pure TiO_2 (this will be discussed in detail hereinafter). Similarly, n_L should be selected among the possible compounds (acetone, isopropanol, diisopropyl ether or propene). Since propene and isopropanol exhibit the lowest and highest indices ($n_{C_3H_6} = 1.36$ and $n_{C_3H_8O} = 1.38$[59]) they have been chosen to validate Eq. (8). Both parameters lead to a relatively good fitting of the experimental data. The $n_{C_3H_8O}$ leads however to a closer fitting. It confirms therefore the chemical analyses (XPS and FTIR). The layer shrinkage originates mainly from the extraction of isopropoxide ligands that have most likely been protonated to isopropanol.

The ligand release occurs only if sufficient energy is supplied to the system. The fraction of thickness loss is plotted against the annealing temperature on Figure 8d for two deposition temperatures. In both cases f_t is proportional to T_a and reaches a plateau that depends on T_{ALD}, i. e. the initial amount of embedded ligands. The extrapolation of the lines for low T_a leads to the same value. This specific temperature, denoted T_{ext} for extraction temperature, is around 80°C. For lower heating conditions no ligands are taken out of the film.

Porosity of the films

It has been mentioned previously that n varies if the composition, the crystalline structure and/or the porosity of the probed material changes. The results shown above indicate that the ligand removal occurring during the thermal treatment (i. e. a composition modification) strongly influences n. Conversely, Figure 9 shows that the refractive index difference ($\Delta n = n - n_0$) is very small (less than 0.02) when the amorphous-to-anatase transition proceeds. The porosity of the film has thus been investigated by EEP. Figure 10a shows the refractive index plotted against RH for various deposition parameters. Note that the samples were heated at 250°C for 5 min to evacuate the potential pores. The effect of such short

treatment on n can be neglected. As previously described,[29] the curves plotted on Figure 10a can roughly be considered as adsorption/desorption isotherms. Though the EEP has been carried out at $\lambda = 600$ nm (instead of 633 nm for the previous ellipsometric investigations), the relative evolution of n at RH $= 0$ is in line with the measurements presented in Figure 8a. For as-deposited TiO_2 grown using TDMAT, $n = 2.48$, rising up to 2.55 after the annealing. In the case of TTIP, n is 2.14, 2.18 and 2.21 for as-deposited layers grown at $T_{ALD} = 120°C$ and annealed layers grown at $T_{ALD} = 80$ and 120°C, respectively.

No evolution against RH is observed when the TiO_2 is deposited with TDMAT or TTIP at high temperature ($T_{ALD} = 200°C$). This points out that those films are not porous. In contrast the isotherms evolve with RH in the case of films deposited at lower temperatures using TTIP. This suggests that those layers are slightly porous. Two different types of isotherms are observed. For TTIP-AG, the curve corresponds to a type I isotherm suggesting narrow cylindrically-shaped pores. Since the n variation remains low, it is not possible to apply the model developed before[29] to extract a rigorous pore size distribution. One can however mention that the pore diameter should be less than 2 nm. A clear hysteresis is observed between the adsorption and desorption measurements for the annealed samples ($T_{ALD} = 80$ and 120°C). These curves fit with a type IV isotherm that is related to ink-bottle-shaped pores exhibiting a larger diameter (ca. 2-6 nm). This is in agreement with the depressions observed in the anatase lattice on the TEM cross section shown in Figure 5.

The comparison of the Δn evolution with RH for those three types of films is shown in Figure 10b and gives additional information on the pore geometry. At $T_{ALD} = 120°C$, Δn_{max} (the difference between the final and the initial refractive index difference) decreases from 0.025 to 0.010 after the annealing. This corresponds to a diminution of the adsorbed volume indicating a lower porosity. This observation is, of course, in agreement with the film thickness shrinkage reported above. Nevertheless the hysteresis measured after the thermal treatment reveals larger pores exhibiting an ink-bottle shape. Such evolution of the film is schematically described on Figure 11a and 11b. The modification of the pore morphology

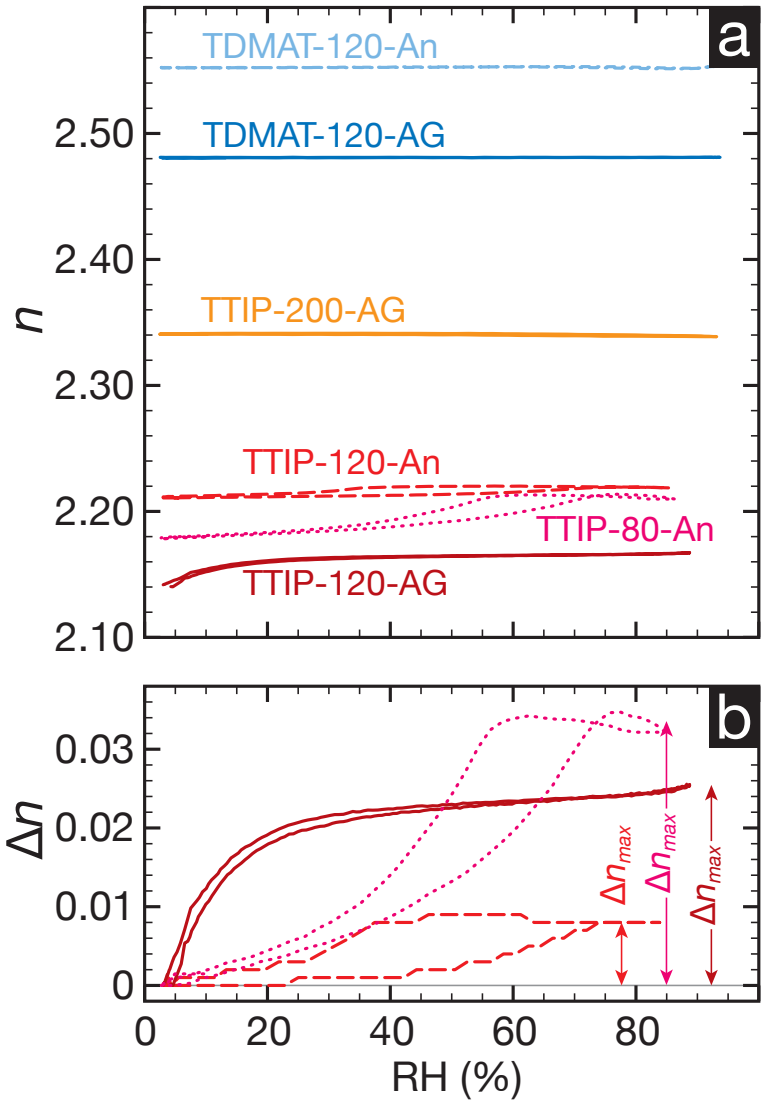

Figure 10: (a) Evolution of n against relative humidity (RH) for TiO_2 layers grown using TTIP and TDMAT. The conditions are indicated on the plots: T_{ALD} and if an annealing at 450°C for 2 h has been performed (An) or not (AG). (b) Relative evolution of n for TTIP-120-AG, TTIP-120-An and TTIP-80-AG. Here n is calculated at $\lambda = 600$ nm.

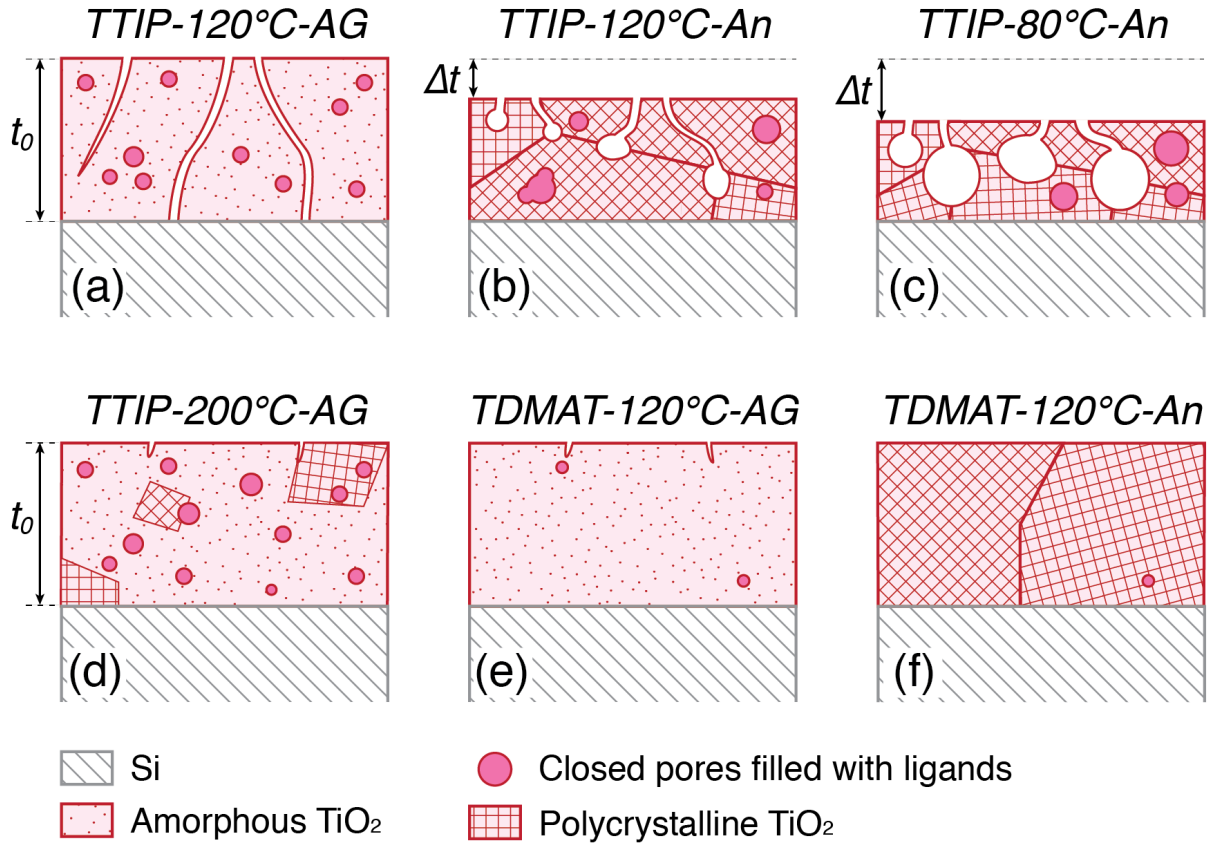

Figure 11: Schematic view of the TiO_2 layers depending on the precursor used during the ALD (TTIP or TDMAT) and if an annealing at 450°C for 2 h has been performed (An) or not (AG). The conditions are indicated on the drawings.

can be ascribed to the coalescence of the tubular narrow pores to form ink-bottle shaped pores that minimize the surface energy of the pores. The effective area of a sphere is indeed lower than that of one or several cylinders, as long as the length of the pores is at least two times greater than the radius. Such pore merging is likely to occur preferentially at grain boundaries. This effect is further enhanced on films grown at $T_{\mathrm{ALD}} = 80°\mathrm{C}$ because the initial amount of trapped ligands is larger. The resulting pores are therefore wider and after annealing the cavities as well as the thickness shrinkage are larger (see Figure 11c). No contact between the ink-bottled shape pores and the underlying Si are drawn on the schemes (Figure 11b and 11c) because after annealing it has been shown, in Figure 2, that the films are stable while a contact is possible between KOH and the Si for TTIP-AG deposited at $T_{\mathrm{ALD}} = 120°\mathrm{C}$ (Figure 11a). The closed porosity is also plotted on Figure 11. It contains trapped ligands that cannot be extracted during the thermal treatment and causes the limitation of the refractive index evolution during the annealing as seen on Figure 8d.

For TDMAT, n is slightly improved with T_{ALD} and also with the annealing. However no porosity is detected and the film is fully stable on immersion in KOH. This indicates that just a small amount of ligands (likely dimethylamine) is also trapped in the layer and its proportion decreases with T_{ALD}. Since no porosity is measured, the amine is removed during the annealing but the concentration is so low that the voids left by the ligands are filled by TiO_2. The n increase could also be ascribed to larger single crystalline domains using this precursor rather than TTIP.

Chemical mechanism of growth

The deposition rate in ALD (i. e. the GPC) is known to depend to a great degree on the saturating coverage of precursor fragments at the end of each precursor pulse,[60] which in turn depends on the extent to which ligand elimination reactions go to completion in each pulse, dictated either by kinetics or by the availability of co-reagents on the surface. Another factor is the steric demand of the ligands; in a previous report, Ritala et al.[9] have explained

the higher GPC for $Ti(OEt)_4$ as compared to TTIP by considering the steric hindrance of the two alkoxides. To test this, we computed the van der Waals volume of the DFT-optimized structures of the precursor molecules (Figure 12) and their protonated ligands. The computed volume of TDMAT is 220.4 $Å^3$ and TTIP is 23% larger (266.9 $Å^3$). The computed volume of the protonated dimethylamine ligand is 55.7 $Å^3$ and the protonated ligand isopropanol is 21% larger (68.7 $Å^3$), meaning that each is a quarter of the volume of the respective entire precursor, as expected. Assuming the hexagonal close-packing of a monolayer of identical spherical ligands with these volumes on a flat surface therefore yields a maximum coverage of 5.1 ligands·nm^{-2} for the ligands of TDMAT and a 13% lower coverage (4.5 ligands·nm^{-2}) for the larger ligands of TTIP (see Supplementary Information). From steric factors alone we would therefore predict a 13% lower ALD growth rate for TTIP relative to TDMAT, which does not account for the substantial differences shown in Figure 1. Instead, it is likely that differences in the extent of ligand elimination are responsible, and this is quantified below.

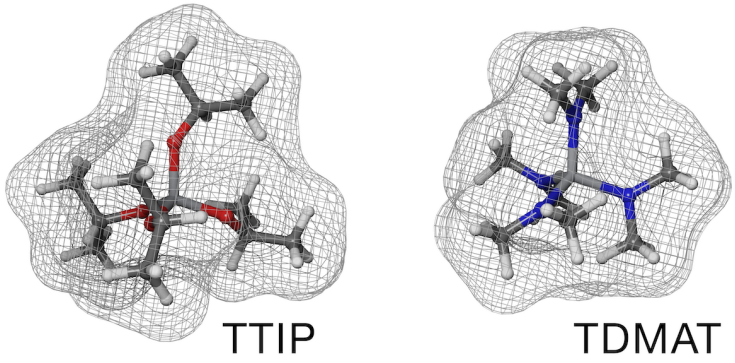

Figure 12: Connolly surfaces mapping the closest approach of a probe sphere (1.4 Å radius) to the van der Waals surface of the two precursor molecules TTIP and TDMAT in their optimum structures computed with DFT; the van der Waals volumes are 266.9 and 220.4 $Å^3$ for TTIP and TDMAT, respectively.

Having accumulated substantial experimental evidence for the incorporation of isopropanol or isopropoxide in the as-deposited films from TTIP, we now proceed to analyze the thickness data in Figure 1 so as to determine whether they are consistent with the expected mechanisms of ALD, described in the following half reactions, where * denotes the surface

species and *? denotes species that may remain at the surface or may desorb. For simplicity, the elimination of only one ligand per Ti during the Ti pulse is given; the actual number eliminated is determined later. For TTIP and water:

$$\mathrm{Ti(OCH(CH_3)_2)_4 + TiO_2{-}OH^* \longrightarrow HOCH(CH_3)_2^{*?} + TiO_2{-}O{-}Ti(OCH(CH_3)_2)_3^*} \quad (9)$$

$$\mathrm{TiO_2{-}O{-}Ti(OCH(CH_3)_2)_3^* + 2\,H_2O \longrightarrow TiO_2{-}TiO_2{-}OH^* + 3\,(HOCH(CH_3)_2)} \quad (10)$$

For TDMAT and water:

$$\mathrm{Ti(N(CH_3)_2)_4 + TiO_2{-}OH^* \longrightarrow HN(CH_3)_2^{*?} + TiO_2{-}O{-}Ti(N(CH_3)_2)_3^*} \quad (11)$$

$$\mathrm{TiO_2{-}O{-}Ti(N(CH_3)_2)_3^* + 2\,H_2O \longrightarrow TiO_2{-}TiO_2{-}OH^* + 3\,HN(CH_3)_2} \quad (12)$$

The mass density of anatase measured in this study ($3.69\,\mathrm{g{\cdot}cm^{-3}}$) can be reformulated as a molar density (ρ=27.8 $\mathrm{TiO_2{\cdot}nm^{-3}}$) and monolayer thickness ($t_{\mathrm{ML}} = 1/\sqrt[3]{\rho} = 3.30\,\text{Å}$). For the annealed samples that have been assigned as anatase, dividing the GPC by t_{ML} thus gives the number of monolayers apparently deposited in each cycle by ALD and these data are given in Table 2. Quite different apparent growth rates are seen for TTIP (0.08-0.17 ML/cycle) and TDMAT (0.26-0.18 ML/cycle with increasing temperature), but as we will now show, an important factor has been neglected.

If ligands persist at the surface (whether as isopropoxide or isopropanol) during the entire ALD process, they will poison a portion of the TiO_2 surface and prevent ALD from taking place (such ALD inhibition has been reported earlier[61] by pulsing various compounds during the process and it is used to modulate the GPC). The fraction of the surface that is active for ALD growth is given by the ratio of the annealed to as-deposited GPC (detailed explanation in Supplementary Information), which, as shown in Table 2, increases for TTIP from 57% to 100% with temperature, but is always at or near 100% for TDMAT. Using this fraction, the number of monolayers per cycle deposited in the active area only can be determined,

and this reveals a drop in ALD growth rate with temperature that is consistent across both TTIP (0.24-0.17 ML/cycle) and TDMAT (0.26-0.18 ML/cycle, Table 2).

In a similar way (see Supplementary Information) the coverage of Ti atoms deposited per unit of active area in each Ti precursor pulse of the ALD cycle can be determined and ranges 2.2-1.6 TiO_2 per nm^2 for TTIP and 2.4-1.6 TiO_2 per nm^2 for TDMAT. We have previously presented the maximum coverage of ligands per unit area based on their size (4.5 and 5.1 per nm^2 for alkoxide and amide, respectively). Combining these two coverages, we can estimate the maximum number of ligands remaining bound to each Ti atom in the fragments on the surface at the end of the Ti pulse. As shown in Table 2, for TTIP this value increases from an average of 2 ligands per Ti atom at 70°C to all 4 ligands still on each Ti atom at 150 and 200°C. The monitoring of this process by quadrupole mass spectrometry (QMS) has also shown that less ligands are removed during the TTIP pulse when the T_{ALD} is increased.[55] The trend is similar but less striking for TDMAT: 2 ligands per Ti at 90°C to 3 ligands per Ti at 150°C. Two ligands per Ti corresponds to fragments $–Ti(OCH(CH_3)_2)_2$ or $–Ti(N(CH_3)_2)_2$ on the surface, although in the real situation it is likely that there is a mix of various fragments with this average composition overall. There is one anomalous data point (4.4 ligands/Ti at 150°C for TTIP), which suggests that the maximum coverage of close-packed ligands is higher than what is actually possible on a real surface.

Table 2: Growth rates, coverages and stoichiometric ratios derived from the experimental GPC data (Figure 1) so as to analyze the growth mechanism. More information is available in the Supplementary Information about how each column is calculated.

Precursor	T_{ALD} (°C)	GPC as-grown (Å/cycle)	GPC annealed (Å/cycle)	Annealed anatase deposited (ML/cy.)	Fraction of surface active for growth (%)	Annealed anatase deposited on active surface (TiO_2/nm^2/cy.)	Annealed anatase deposited on active surface (ML/cy.)	Maximum ligand stoichiometry at active surface after Ti pulse (Ligand/Ti)	OH reacting at surface during Ti pulse (OH/nm^2/cy.)	Protonated ligands incorporated (LigandH/nm^2/cy.)	Stoichiometry of incorporation of protonated ligands (LigandH/Ti)
TTIP	70	0.45	0.26	0.08	57.8	2.16	0.24	2.1	4.18	0.28	0.38
	80	0.42	0.28	0.08	66.7	1.75	0.19	2.6	2.53	0.20	0.26
	90	0.36	0.25	0.08	69.4	1.44	0.16	3.1	1.29	0.16	0.23
	120	0.35	0.29	0.09	82.9	1.17	0.13	3.8	0.22	0.09	0.11
	150	0.33	0.30	0.09	90.9	1.01	0.11	4.4	-0.44	0.04	0.05
	200	0.39	0.39	0.12	100.0	1.08	0.12	4.1	-0.14	0.00	0.00
	250	0.57	0.57	0.17	100.0	1.58	0.17	2.8	1.86	0.00	0.00
TDMAT	90	0.86	0.85	0.26	98.8	2.42	0.26	2.1	4.52	0.02	0.01
	120	0.65	0.65	0.20	100.0	1.81	0.20	2.8	2.08	0.00	0.00
	150	0.58	0.58	0.18	100.0	1.61	0.18	3.2	1.30	0.00	0.00

Nevertheless, the above analysis is consistent with the ideal mechanism of ALD on the active surface for 70-200°C, whereby during the Ti pulse, the TTIP or TDMAT precursor adsorbs to a hydroxylated TiO_2 surface and loses a portion of its ligands by a Brønsted acid-base reaction, yielding protonated ligands that usually desorb. In the ideal mechanism, the remaining ligands are eliminated during the subsequent H_2O pulse and the hydroxylated surface is restored. The substantially higher GPC for TTIP at 250°C gives values in Table 2 that are inconsistent with the trend, suggesting additional non-ALD deposition at this temperature, probably due to thermal decomposition of ligands. Such phenomenon has been previously reported for CVD and ALD.[55,62]

Also quoted in Table 2 is the coverage of hydroxyl groups that evidently react with ligands in the Ti pulse. The observed decrease of this OH coverage with temperature is consistent with the trend of decreasing equilibrium coverage of OH on titania surfaces as temperature is increased.[63] Since TTIP and TDMAT processes give different coverages of reactive OH groups in Table 2 at any given temperature, it is likely that the actual OH coverage at the end of the H_2O pulse is somewhat higher than the values given here, but that not all of these OH are reactive with the respective ligands during the Ti pulse.

It is now possible to explain the difference in GPC between TTIP and TDMAT as being due to differences in the extent of the ALD reaction during the Ti pulse. At the lowest temperatures (70°C for TTIP, 90°C for TDMAT), two ligands are eliminated from each precursor during the Ti pulse in both processes, leaving fragments with an average of two ligands per Ti. The availability of protons at the titania surface decreases with temperature. At and above 150°C no ligands can be protonated and eliminated from TTIP during the TTIP pulse, resulting in a low coverage of adsorbed Ti. This is not fully in line with previous QMS and quartz microbalance experiments, reported by Rahtu and Ritala,[55] indicating that some ligand removal is still detected between 150 and 200°C. Although the calculations are not in complete agreement with the QMS data, in both cases the number of reacting ligands during the TTIP pulse decreases with T_{ALD}. The discrepancy can arise from various factors.

In their study, Rahtu and Ritala[55] have maybe overestimated the number of released ligands since they consider that, after each cycle, uncontaminated TiO_2 is grown while the ligand trapping is considered in the present work. According to the authors, the geometry of the reactor as well as the residence time (that is very long in our process) can also modify significantly the decomposition of the precursors.[55,64,65] By contrast, at 150°C for TDMAT, an average of one ligand per precursor is still eliminated, which frees up space at the surface and allows a higher coverage of Ti to adsorb, though still less than at 90°C. In other words, the ALD reaction proceeds further towards completion during the TDMAT pulse than during the TTIP pulse. This indicates higher reactivity of the alkylamide ligand with the hydroxyl groups of titania. The higher reactivity of amides relative to alkoxides in Ti precursors for oxide ALD has been predicted before using DFT.[66]

For both precursors, we therefore explain the decrease in ALD growth rate with temperature as ultimately due to the decrease in OH coverage on TiO_2 after the water pulse. (The apparent ALD window for TTIP is in fact the consequence of less ligand incorporation being counter-balanced by less availability of OH).

The difference between as-deposited and annealed GPCs also allows us to quantify the amount of ligand or protonated ligand that may have been incorporated into the as-deposited film and removed on annealing. To do this, the volume lost on annealing is divided by the computed volume per ligand or protonated ligand (which are the same to within 1%). The resulting coverage of protonated ligands is again compared with the coverage of Ti deposited, revealing that 0.38 isopropanol ligands are incorporated per Ti atom from TTIP at 70°C, just 0.11 isopropanol/Ti at 120°C and zero at 200°C (Table 2). Some uncertainty remains over the chemical nature of the incorporated ligand. One possibility is that a fraction of the protonated by-product isopropanol fails to desorb and is incorporated as the film grows. If this is the case, then we find that 91% of the TTIP by-product desorbs during ALD at 70°C and 97% desorbs at 120°C. As noted above, this decrease is probably due to evaporation of more isopropanol with increased temperature. Alternatively, the ligand may persist

as the unprotonated isopropoxide anion, kinetically inert towards H_2O because of the local geometry. This has previously been computed with DFT[67] and detected experimentally[68,69] for ALD of other oxides, albeit without ligand incorporation into the film. In either case, because of their size, the small number of incorporated ligands has a disproportionately large effect - blocking ALD on a portion of the surface, swelling the apparent thickness deposited and leaving behind pores after annealing, thus affecting quite substantially the morphology, stability and electrical properties of the film.

We now address the question of whether carbonaceous impurities are always indicative of CVD. Isopropanol is the by-product from TTIP of the standard Brønsted acid-base reactions of water-based ALD. The failure of some ligand or by-product to desorb at low temperature does not affect the self-limiting nature of the ALD reactions, as indicated by the consistency of the analysis in Table 2. Indeed, the deliberate or adventitious blocking of the surface by persistent ligands seems to be quite widespread in ALD processes.[70] This means that, although C is incorporated into the film, the TTIP process may still be described as self-limiting ALD (as proposed by Elam et al.[61]) and should consequently show excellent conformality. Clearly though, the occurence of pores after annealing means that film quality from the TTIP process is not as good as that from TDMAT, which is apparently closer to an ideal ALD process. Finally, for TTIP-AG at 120°C we note that the calculated value of 0.10 ligands incorporated per TiO_2 can be re-formulated as 0.05 (i. e. 5%) ligand-O atoms per titania-O atoms deposited. This agrees with the experimental finding of 5% higher O_{II}+O_{III} XPS signals in TTIP-AG relative to TTIP-An, as presented above.

Electrical properties

The present study shows the strong correlation between the Ti precursor chemistry and process temperature on one side and the composition and morphology of the film on the other side. However, it is even more significant to assess the impact of those parameters on the properties and thus on the technological applications of the layers. Since TiO_2 exhibits a high

dielectric constant the insulating properties of the films have been measured depending on the deposition conditions in MOS configuration. Figure 13a shows the evolution of the leakage current density (j) with the applied voltage (U). Several indications can be extracted from the comparison of j. For layers deposited with TTIP, the annealing lowers the leakage current and a better dielectric behavior is observed at high T_{ALD} ($j_{200^\circ\mathrm{C}} = 10^{-3}\,\mathrm{A{\cdot}cm^{-2}}$ at $U = 1\,\mathrm{V}$). Using TDMAT allows the best electrical performance to be reached ($j = 8{\times}10^{-5}\,\mathrm{A{\cdot}cm^{-2}}$ at $U = 1\,\mathrm{V}$). The present values are very interesting since they are better than those reported in literature[11] where 10 nm thick films deposited by thermal and PE-ALD using TDMAT exhibit higher leakage currents: $j = 5{\times}10^{-3}$ and $7{\times}10^{-4}\,\mathrm{A{\cdot}cm^{-2}}$, respectively. Note that those layers were thinner (10 nm instead of 40 nm in the present study) and the leakage current can also strongly vary with the contact area.[71] The main information of Figure 13a is the direct correlation between the dielectric properties and the refractive index. The insulating efficiency is indeed better when n is higher. This is further illustrated in Figure 13b where j is plotted against n at three different U for different ALD conditions. It shows that porous layers or films containing a large amount of incorporated ligands exhibit poor dielectric properties. In a previous work,[28] a transition from n-type to p-type behavior was reported after annealing in N_2 or O_2 at $T_a > 600^\circ$C. Such conversion was ascribed to the variation of the concentration of oxygen interstitials. In the current study, the XPS analyses give the oxygen content in the TiO_2 around 21.5% for TTIP-AG and around 15.5% for the other cases (see Table 1). The highest leakage current is measured for TTIP-AG. This could be expected for a p-type semiconductor positively biased. However, the strong differences observed between the other leakage currents (TTIP-AG-200°C, TTIP-An-120°C, and TDMAT-AG-150°C) can barely not be explained similarly since the oxygen concentration does not vary from one to another. The different electric behavior is more likely related to the ligand content and/or the porosity of the films depending on their deposition conditions. The present result confirms that the refraction index is an accurate indicator of the quality of such ALD thin films.

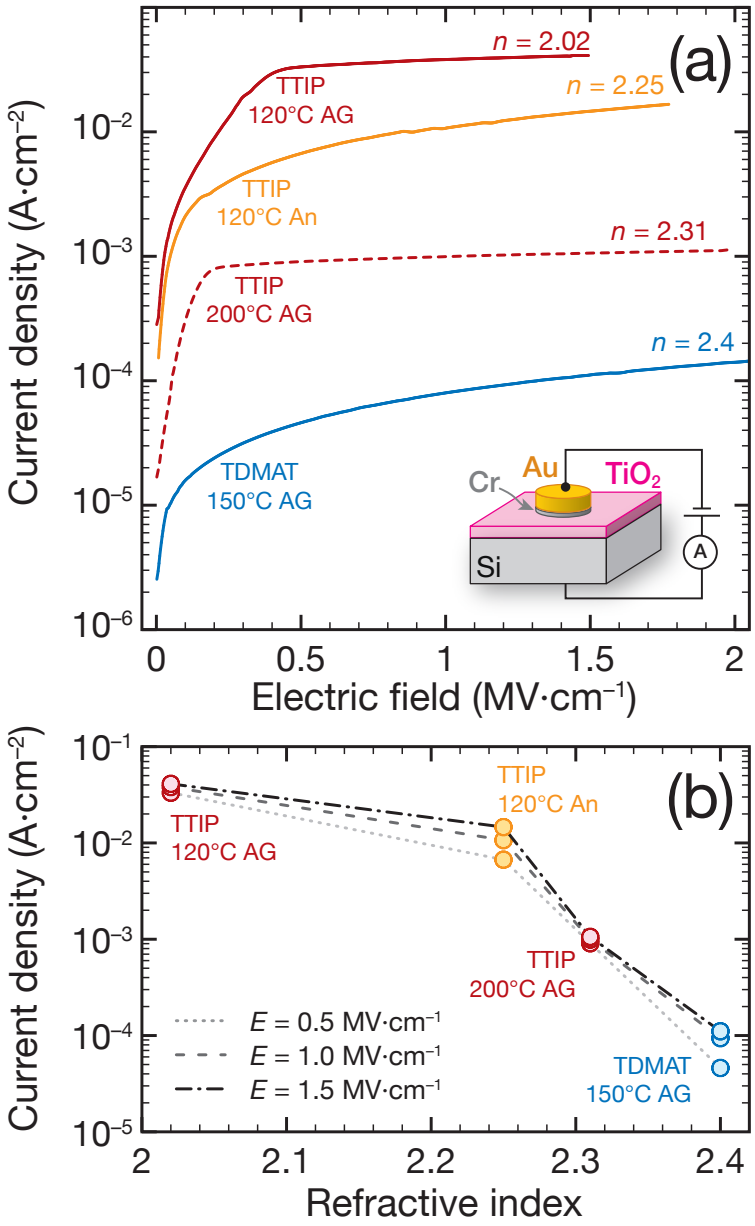

Figure 13: (a) Leakage current densities vs electric field of TiO_2 thin films grown on n-type Si using TTIP ($T_{ALD} = 120$ and 200°C) with and without annealing ($T_a = 450$°C for 2 h) and using TDMAT ($T_{ALD} = 150$°C). The corresponding refraction index at $\lambda = 633$ nm is indicated on the plot. The inset displays a schematic of the measurement setup. (b) Leakage current densities vs refractive index at various electric field: $E = 0.5$, 1.0 and 1.5 MV·cm^{-1}.

Conclusion

This is the first time that a significant thickness shrinkage in ALD TiO_2 thin films after annealing has been reported and explained. The effect was observed only with the TTIP precursor and water at low process temperatures and not with TDMAT and water, and is correlated to a strong instability when the coating was in contact with KOH. This unexpected observation has been investigated through a comprehensive physico-chemical characterization of the layers as a function of the ALD conditions, which has led to a better understanding of the growth mechanism. XPS, FTIR and ellipsometric investigations have revealed the critical effect of the precursor nature on the chemical composition of the TiO_2 layers. This study also demonstrates that the refractive index is a very accurate indicator of the quality of TiO_2 thin films. In the case of TDMAT, an almost pure and highly compact film was deposited at process temperatures between 90 and 150°C consistent with a standard ALD mechanism. The decrease of growth rate with temperature is ascribed to a decrease in availability of surface hydroxyl groups on TiO_2 after the water pulse. This results in a decrease in the proportion of amine ligands eliminated during the TDMAT pulse - from half at 90°C down to a quarter at 150°C according to DFT-computed structures - and consequently in less Ti adsorbing in each ALD cycle. Qualitatively similar behavior was seen for the TTIP precursor at 150-200°C, albeit with a lower deposition rate due to the lower reactivity of the alkoxide ligands, which are eliminated exclusively during the water pulse. The higher deposition rate with TTIP above 200°C appears to be due to non-ALD reactions. However, using TTIP below 150°C, the consistent picture that emerges from the various characterization techniques is of some of the isopropanol by-product (of self-limiting ALD) failing to desorb and being incorporated into the film as it grows. Although relatively little by-product is incorporated (9% at 70°C, dropping to 1% at 150°C), these trapped ligands occupy significant volume, preventing ALD on a portion of the surface and also swelling the thickness of the as-deposited film. The trapped ligands can be quickly removed by annealing, leading to shrinkage of the film, though the properties of pure TiO_2 cannot be entirely recovered. This

is because, when extracted by heating or immersion in aqueous solution, the ligands leave behind tiny tubular pores in the film, which can be changed to ink-bottle shaped pores by the thermal treatment. We therefore explain how retention of alkoxide ligands during film growth at temperatures lower than 200°C can be a characteristic of self-limiting ALD and how it can have a lasting effect on film morphology and properties.

Acknowledgement

The authors are grateful to F. Bedu, D. Chaudansson, V. Heresanu, S. Lavandier and A. Ranguis (CINaM) for their meticulous help for clean-room processing, electron microscopy assistance, X-ray diffraction analysis, electrical measurements and AFM observations. Prof. J.-M. Raimundo (CINaM) is also acknowledged for fruitful discussions. M. W. Diouf and M. E. Dufond are indebted to the Région Sud Provence-Alpes-Côte d'Azur, Encapsulix SAS and to the Ministry of Higher Education, Research and Innovation (Doctoral School ED352 of the Aix-Marseille Univ.), respectively for the PhD grants.

Supporting Information Available

Details on the calculation of ligand coverage from volume and calculation of of chemical mechanism of growth. GPC as function of the pulse duration of the different precursors. AFM top views of TiO_2 thin films grown on Si wafers. Comparisons of the evolution of the GPCs found in literature. X-ray reflectivity of TiO_2 layers grown using TDMAT before and after annealing. X-ray diffractograms of TiO_2 layers grown using TTIP depending on T_a and T_{ALD} XPS survey spectra of TiO_2 thin films depending on the Ti precursor (TTIP or TDMAT) and prior and after annealing. TEM cross sections at low and high resolutions of TDAMT-AG.

This material is available free of charge via the Internet at `http://pubs.acs.org/`.

References

(1) Chen, X.; Mao, S. S. Titanium Dioxide Nanomaterials: Synthesis, Properties, Modifications, and Applications. *Chem. Rev.* **2007**, *107*, 2891–2959.

(2) Reiners, M.; Xu, K.; Aslam, N.; Devi, A.; Waser, R.; Hoffmann-Eifert, S. Growth and Crystallization of TiO_2 Thin Films by Atomic Layer Deposition Using a Novel

Amido Guanidinate Titanium Source and Tetrakis-dimethylamido-titanium. *Chem. Mater.* **2013**, *25*, 2934–2943.

(3) Martin, N.; Rousselot, C.; Rondot, D.; Palmino, F.; Mercier, R. Microstructure modification of amorphous titanium oxide thin films during annealing treatment. *Thin Solid Films* **1997**, *300*, 113–121.

(4) Macwan, D. P.; Dave, P. N.; Chaturvedi, S. A review on nano-TiO2 sol–gel type syntheses and its applications. *J Mater Sci* **2011**, *46*, 3669–3686.

(5) Sveshnikova, G. S.; Koltsov, S. I.; Aleskovskii, V. B. Interaction of titanium tetrachloride with hydroxylated silicon surfaces. *J. Appl. Chem. USSR* **1970**, *43*, 432–434.

(6) Lakomaa, E. L.; Haukka, S.; Suntola, T. Atomic layer growth of TiO2 on silica. *Appl Surf Sci* **1992**, *60-61*, 742–748.

(7) Ritala, M.; Leskelä, M.; Niinisto, L.; Haussalo, P. Titanium isopropoxide as a precursor in atomic layer epitaxy of titanium dioxide thin films. *Chem. Mater.* **1993**, *5*, 1174–1181.

(8) Aarik, J.; Aidla, A.; Uustare, T.; Ritala, M.; Leskelä, M. Titanium isopropoxide as a precursor for atomic layer deposition: characterization of titanium dioxide growth process. *Appl. Surf. Sci.* **2000**, *161*, 385–395.

(9) Ritala, M.; Leskelä, M.; Rauhala, E. Atomic layer epitaxy growth of titanium dioxide thin films from titanium ethoxide. *Chem. Mater.* **1994**, *6*, 556–561.

(10) Schuisky, M.; Hårsta, A.; Aidla, A.; Kukli, K.; Kiisler, A.-A.; Aarik, J. Atomic Layer Chemical Vapor Deposition of TiO_2 Low Temperature Epitaxy of Rutile and Anatase. *J. Electrochem. Soc.* **2000**, *147*, 3319–7.

(11) Maeng, W. J.; Kim, H. Thermal and Plasma-Enhanced ALD of Ta and Ti Oxide Thin Films from Alkylamide Precursors. *Electrochem. Solid-State Lett.* **2006**, *9*, G191–4.

(12) Lim, G. T.; Kim, D.-H. Characteristics of TiOx films prepared by chemical vapor deposition using tetrakis-dimethyl-amido-titanium and water. *Thin Solid Films* **2006**, *498*, 254–258.

(13) Xie, Q.; Jiang, Y.-L.; Detavernier, C.; Deduytsche, D.; Van Meirhaeghe, R. L.; Ru, G.-P.; Li, B.-Z.; Qu, X.-P. Atomic layer deposition of TiO2 from tetrakis-dimethyl-amido titanium or Ti isopropoxide precursors and H2O. *J. Appl. Phys.* **2007**, *102*, 083521–6.

(14) Lee, J. P.; Park, M. H.; Chung, T. M.; Kim, Y.; M, S. M. Atomic Layer Deposition of TiO_2 Thin Films from $Ti(OiPr)_2(dmae)_2$ and H_2O**âĂĺ**. *Bulletin of the Korean Chemical Society* **2004**, *25*, 471–475.

(15) Gebhard, M.; Mitschker, F.; Wiesing, M.; Giner, I.; Torun, B.; de los Arcos, T.; Awakowicz, P.; Grundmeier, G.; Devi, A. An efficient PE-ALD process for TiO_2 thin films employing a new Ti-precursor. *Journal of Materials Chemistry C* **2016**, *4*, 1057–1065.

(16) Rose, M.; Niinistö, J.; Michalowski, P.; Gerlich, L.; Wilde, L.; Endler, I.; Bartha, J. W. Atomic Layer Deposition of Titanium Dioxide Thin Films from Cp*Ti(OMe) 3and Ozone. *J. Phys. Chem. C* **2009**, *113*, 21825–21830.

(17) Blanquart, T.; Niinistö, J.; Gavagnin, M.; Longo, V.; Pallem, V. R.; Dussarrat, C.; Ritala, M.; Leskelä, M. Novel Heteroleptic Precursors for Atomic Layer Deposition of TiO_2. *Chem. Mater.* **2012**, *24*, 3420–3424.

(18) King, D. M.; Liang, X.; Zhou, Y.; Carney, C. S.; Hakim, L. F.; Li, P.; Weimer, A. W. Atomic layer deposition of TiO2 films on particles in a fluidized bed reactor. *Powder Technology* **2008**, *183*, 356–363.

(19) Rai, V. R.; Agarwal, S. Surface Reaction Mechanisms during Ozone-Based Atomic Layer Deposition of Titanium Dioxide. *J. Phys. Chem. C* **2008**, *112*, 9552–9554.

(20) Cleveland, E. R.; Henn-Lecordier, L.; Rubloff, G. W. Role of surface intermediates in enhanced, uniform growth rates of TiO 2atomic layer deposition thin films using titanium tetraisopropoxide and ozone. *J. Vac. Sci. Technol. A* **2012**, *30*, 01A150–6.

(21) Lim, J. W.; Yun, S. J.; Lee, J. H. Characteristics of TiO_2 Films Prepared by ALD With and Without Plasma. *Electrochem. Solid-State Lett.* **2004**, *7*, F73–4.

(22) Aghaee, M.; Maydannik, P. S.; Johansson, P.; Kuusipalo, J.; Creatore, M.; Homola, T.; Cameron, D. C. Low temperature temporal and spatial atomic layer deposition of TiO_2 films. *J. Vac. Sci. Technol. A* **2015**, *33*, 041512–9.

(23) Avril, L.; Reymond-Laruinaz, S.; Decams, J. M.; Bruyère, S.; Potin, V.; de Lucas, M. C. M.; Imhoff, L. TiO2 anatase films obtained by direct liquid injection atomic layer deposition at low temperature. *Appl. Surf. Sci.* **2014**, *288*, 201–207.

(24) Wu, Y.; Döhler, D.; Barr, M.; Oks, E.; Wolf, M.; Santinacci, L.; Bachmann, J. Atomic Layer Deposition from Dissolved Precursors. *Nano Lett.* **2015**, *15*, 6379–6385.

(25) Niemelä, J.-P.; Marin, G.; Karppinen, M. Titanium dioxide thin films by atomic layer deposition: a review. *Semicond. Sci. Technol.* **2017**, *32*, 093005–71.

(26) Zydor, A.; Kessler, V. G.; Elliott, S. D. First principles simulation of reaction steps in the atomic layer deposition of titania: dependence of growth on Lewis acidity of titanocene precursor. *Phys. Chem. Chem. Phys.* **2012**, *14*, 7954–11.

(27) Shirazi, M.; Elliott, S. D. Multiple Proton Diffusion and Film Densification in Atomic Layer Deposition Modeled by Density Functional Theory. *Chem. Mater.* **2013**, *25*, 878–889.

(28) Iancu, A. T.; Logar, M.; Park, J.; Prinz, F. B. Atomic Layer Deposition of Undoped TiO_2 Exhibiting p-Type Conductivity. *ACS Appl. Mater. Interfaces* **2015**, *7*, 5134–5140.

(29) Boissière, C.; Grosso, D.; Lepoutre, S.; Nicole, L.; Bruneau, A. B.; Sanchez, C. Porosity and Mechanical Properties of Mesoporous Thin Films Assessed by Environmental Ellipsometric Porosimetry. *Langmuir* **2005**, *21*, 12362–12371.

(30) Bochevarov, A. D.; Harder, E.; Hughes, T. F.; Greenwood, J. R.; Braden, D. A.; Philipp, D. M.; Rinaldo, D.; Halls, M. D.; Zhang, J.; Friesner, R. A. Jaguar: A high-performance quantum chemistry software program with strengths in life and materials sciences. *Int. J. Quantum Chem.* **2013**, *113*, 2110–2142.

(31) Perdew, J. P.; Burke, K.; Ernzerhof, M. Generalized Gradient Approximation Made Simple [Phys. Rev. Lett. 77, 3865 (1996)]. *Phys. Rev. Lett.* **1997**, *78*, 1396–1396.

(32) Perdew, J. P.; Burke, K.; Ernzerhof, M. Generalized Gradient Approximation Made Simple. *Phys. Rev. Lett.* **1996**, *77*, 3865–3868.

(33) Graner, G. The methyl bromide molecule: A critical consideration of perturbations in spectra. *Journal of Molecular Spectroscopy* **1981**, *90*, 394–438.

(34) Roy, L. E.; Hay, P. J.; Martin, R. L. Revised Basis Sets for the LANL Effective Core Potentials. *J. Chem. Theory Comput.* **2008**, *4*, 1029–1031.

(35) Van de Kerckhove, K.; Mattelaer, F.; Deduytsche, D.; Vereecken, P. M.; Dendooven, J.; Detavernier, C. Molecular layer deposition of "titanicone", a titanium-based hybrid material, as an electrode for lithium-ion batteries. *Dalton Trans.* **2015**, *45*, 1176–1184.

(36) Van de Kerckhove, K.; Barr, M. K. S.; Santinacci, L.; Vereecken, P. M.; Dendooven, J.; Detavernier, C. The transformation behaviour of "alucones", deposited by molecular layer deposition, in nanoporous Al_2O_3 layers. *Dalton Trans.* **2018**, *47*, 5860–5870.

(37) Zhang, L.; Jiang, H. C.; Liu, C.; Dong, J. W.; Chow, P. Annealing of Al_2O_3thin films prepared by atomic layer deposition. *J. Phys. D: Appl. Phys.* **2007**, *40*, 3707–3713.

(38) Cimalla, V.; Baeumler, M.; Kirste, L.; Prescher, M.; Christian, B.; Passow, T.; Benkhelifa, F.; Bernhardt, F.; Eichapfel, G.; Himmerlich, M.; Krischok, S.; Pezoldt, J. Densification of Thin Aluminum Oxide Films by Thermal Treatments. *Mater. Sci. Appl.* **2014**, *05*, 628–638.

(39) Richards, B. S. Single-material TiO2 double-layer antireflection coatings. *Solar Energy Materials and Solar Cells* **2003**, *79*, 369–390.

(40) Bendavid, A.; Martin, P. J.; Takikawa, H. Deposition and modification of titanium dioxide thin films by filtered arc deposition. *Thin Solid Films* **2000**, *360*, 241–249.

(41) Qin, M. J.; Kuo, E. Y.; Whittle, K. R.; Middleburgh, S. C.; Robinson, M.; Marks, N. A.; Lumpkin, G. R. Density and structural effects in the radiation tolerance of TiO_2 polymorphs. *J. Phys.: Condens. Matter* **2013**, *25*, 355402–8.

(42) Xie, Q.; Musschoot, J.; Deduytsche, D.; Van Meirhaeghe, R. L.; Detavernier, C.; Van den Berghe, S.; Jiang, Y.-L.; Ru, G.-P.; Li, B.-Z.; Qu, X.-P. Growth Kinetics and Crystallization Behavior of TiO_2 Films Prepared by Plasma Enhanced Atomic Layer Deposition. *J. Electrochem. Soc.* **2008**, *155*, H688–5.

(43) Lee, S. Y.; Jeon, C.; Kim, S. H.; Kim, Y.; Jung, W.; An, K.-S.; Park, C.-Y. In-situ X-ray Photoemission Spectroscopy Study of Atomic Layer Deposition of TiO_2 on Silicon Substrate. *Jpn. J. Appl. Phys.* **2012**, *51*, 031102–3.

(44) Hackler, R. A.; Kang, G.; Schatz, G. C.; Stair, P. C.; Van Duyne, R. P. Analysis of TiO Atomic Layer Deposition Surface Chemistry and Evidence of Propene Oligomerization using Surface-Enhanced Raman Spectroscopy. *J. Am. Chem. Soc.* **2018**, *141*, 414–422.

(45) Reed, P. J.; Mehrabi, H.; Schichtl, Z. G.; Coridan, R. H. Enhanced Electrochemical Stability of TiO2-Protected, Al-doped ZnO Transparent Conducting Oxide Synthesized by Atomic Layer Deposition. *ACS Appl. Mater. Interfaces* **2018**, *10*, 43691–43698.

(46) Singh, A. K.; Adstedt, K.; Brown, B.; Singh, P. M.; Graham, S. Development of ALD Coatings for Harsh Environment Applications. *ACS Appl. Mater. Interfaces* **2018**, *11*, 7498–7509.

(47) Pourbaix, M. *Atlas d'équilibres électrochimiques*; Gauthier-Villars & Cie: Paris, 1963.

(48) Palik, E. D. Ellipsometric Study of Orientation-Dependent Etching of Silicon in Aqueous KOH. *J. Electrochem. Soc.* **1985**, *132*, 871–14.

(49) Ali-Löytty, H.; Hannula, M.; Saari, J.; Palmolahti, L.; Bhuskute, B. D.; Ulkuniemi, R.; Nyyssönen, T.; Lahtonen, K.; Valden, M. Diversity of TiO2: Controlling the Molecular and Electronic Structure of Atomic-Layer-Deposited Black TiO2. *ACS Appl. Mater. Interfaces* **2019**, *11*, 2758–2762.

(50) Santinacci, L.; Diouf, M. W.; Barr, M. K. S.; Fabre, B.; Joanny, L.; Gouttefangeas, F.; Loget, G. Protected Light-Trapping Silicon by a Simple Structuring Process for Sunlight-Assisted Water Splitting. *ACS Appl. Mater. Interfaces* **2016**, *8*, 24810–24818.

(51) Li, W.; Li, L.; Wu, X.; Li, J.; Jiang, L.; Yang, H.; Ke, G.; Cao, G.; Deng, B.; Xu, W. High Infrared Blocking Cellulose Film Based on Amorphous to Anatase Transition of TiO2 via Atomic Layer Deposition. *ACS Appl. Mater. Interfaces* **2018**, *10*, 21056–21060.

(52) Karlsson, P. G.; Richter, J. H.; Andersson, M. P.; Johansson, M. K. J.; Blomquist, J.; Uvdal, P.; Sandell, A. TiO2 chemical vapor deposition on Si(111) in ultrahigh vacuum: Transition from interfacial phase to crystalline phase in the reaction limited regime. *Surface Science* **2011**, *605*, 1147–1156.

(53) Head, A. R.; Johansson, N.; Niu, Y.; Snezhkova, O.; Chaudhary, S.; Schnadt, J.; Bluhm, H.; Chen, C.; Avila, J.; Asensio, M.-C. In situcharacterization of the deposition of anatase TiO_2 on rutile TiO_2(110). *J. Vac. Sci. Technol. A* **2018**, *36*, 02D405–7.

(54) Socrates, G. *Infrared and Raman Characteristic Group Frequencies*, 3rd ed.; John Wiley & Sons Ltd: Baffins Lane, 2001.

(55) Rahtu, A.; Ritala, M. Reaction Mechanism Studies on Titanium Isopropoxide–Water Atomic Layer Deposition Process. *Chem. Vap. Deposition* **2002**, *8*, 21–8.

(56) Carrizosa, I. Study of the interaction of aliphatic alcohols with TiO2 II. On the mechanism of alcohol dehydration on anatase. *Journal of Catalysis* **1977**, *49*, 189–200.

(57) Ratzsch, S.; Kley, E.-B.; Tünnermann, A.; Szeghalmi, A. Influence of the oxygen plasma parameters on the atomic layer deposition of titanium dioxide. *Nanotechnology* **2014**, *26*, 024003–11.

(58) Jin, C.; Liu, B.; Lei, Z.; Sun, J. Structure and photoluminescence of the TiO2 films grown by atomic layer deposition using tetrakis-dimethylamino titanium and ozone. *Nanoscale Res Lett* **2015**, *10*, 2042–9.

(59) Sani, E.; Dell'Oro, A. Spectral optical constants of ethanol and isopropanol from ultraviolet to far infrared. *Optical Materials* **2016**, *60*, 137–141.

(60) Elliott, S. D.; Scarel, G.; Wiemer, C.; Fanciulli, M.; Pavia, G. Ozone-Based Atomic Layer Deposition of Alumina from TMA: Growth, Morphology, and Reaction Mechanism. *Chem. Mater.* **2006**, *18*, 3764–3773.

(61) Yanguas-Gil, A.; Libera, J. A.; Elam, J. W. Modulation of the Growth Per Cycle in Atomic Layer Deposition Using Reversible Surface Functionalization. *Chem. Mater.* **2013**, *25*, 4849–4860.

(62) Siefering, K. L. Kinetics of Low-Pressure Chemical Vapor Deposition of TiO[sub 2] from Titanium Tetraisopropoxide. *J. Electrochem. Soc.* **1990**, *137*, 814–5.

(63) Walle, L. E.; Borg, A.; Johansson, E. M. J.; Plogmaker, S.; Rensmo, H.; Uvdal, P.;

Sandell, A. Mixed Dissociative and Molecular Water Adsorption on Anatase TiO_2(101). *J. Phys. Chem. C* **2011**, *115*, 9545–9550.

(64) Martin, N.; Rousselot, C.; Rondot, D.; Palmino, F.; Mercier, R. Microstructure modification of amorphous titanium oxide thin films during annealing treatment. *Thin Solid Films* **1997**, *300*, 113–121.

(65) Gao, Y. In-situ IR and spectroscopic ellipsometric analysis of growth process and structural properties of Ti1−xNbxO2 thin films by metal-organic chemical vapor deposition. *Thin Solid Films* **1999**, *346*, 73–81.

(66) Murray, C.; Elliott, S. D. Density Functional Theory Predictions of the Composition of Atomic Layer Deposition-Grown Ternary Oxides. *ACS Appl. Mater. Interfaces* **2013**, *5*, 3704–3715.

(67) Mahdi Shirazi, S. D. E. Cooperation between adsorbates accounts for the activation of atomic layer deposition reactions. *Nanoscale* **2015**, *7*, 6311–6318.

(68) Vandalon, V.; Kessels, W. M. M. What is limiting low-temperature atomic layer deposition of Al_2O_3? A vibrational sum-frequency generation study. *Appl. Phys. Lett.* **2016**, *108*, 011607–5.

(69) Mackus, A. J. M.; MacIsaac, C.; Kim, W.-H.; Bent, S. F. Incomplete elimination of precursor ligands during atomic layer deposition of zinc-oxide, tin-oxide, and zinc-tin-oxide. *J. Chem. Phys.* **2017**, *146*, 052802–11.

(70) Vandalon, V.; Kessels, W. M. M. E. Revisiting the growth mechanism of atomic layer deposition of Al_2O_3: A vibrational sum-frequency generation study. *J. Vac. Sci. Technol. A* **2017**, *35*, 05C313–15.

(71) Das, C.; Henkel, K.; Tallarida, M.; Schmeisser, D.; Gargouri, H.; Kärkkänen, I.; Schneidewind, J.; Gruska, B.; Arens, M. Thermal and plasma enhanced atomic layer deposi-

tion of TiO_2: Comparison of spectroscopic and electric properties. *J. Vac. Sci. Technol. A* **2015**, *33*, 01A144–9.

Graphical TOC Entry